SUPPLEMENTARY MATERIALS:

Online Appendix to

Policy Transition Risk, Carbon Premiums, and Asset Prices

Revised version: March 2025

Abstract

Here we present additional material such as proofs, a description of the numerical solution algorithm, calibration details, and further simulation results and robustness checks.

Table of Contents

A Solution Approach

In order to give a unified description of the solution procedure, Appendices A and B show the solution procedure for the extended model of section 5. In particular, the derivations include the three-dimensional Markov chain $\mathbf{X} = (X^p, X^t, X^c)$ and climate-related disasters.

A.1 Hamilton-Jacobi-Bellman Equation

Applying the Bellman principle in continuous time, the value function $J = J(t, K_1, K_2, T, \mathbf{X})$ solves a non-linear partial differential equation, which is typically refered to as Hamilton-Jacobi-Bellman equation (e.g., Duffie and Epstein 1992b). This equation is given by

$$\begin{aligned} 0 = \max_{D, F_n, G_n, I_n, R} \Bigg\{ & J_t + \delta\theta J \Big(\frac{\left(\sum_{n=1,2}[Y_n - I_n - b_g G_n - b_f F_n - \varsigma_n b_d(S, \mathbf{X}, D, K)]\right)^{1-1/\psi}}{[(1-\gamma)J]^{\frac{1-1/\psi}{1-\gamma}}} - 1 \Big) \\ & + J_T \vartheta(\mathbf{X}) \big(\nu_t [F_1 + F_2] - D \big) + \frac{1}{2} J_{TT} \sigma_T^2 + J_{K_1} \Big(I_1 - \frac{1}{2}\phi_1 \frac{I_1^2}{K_1} + R - \frac{1}{2}\kappa \frac{R^2}{K_1} - \delta_1^k K_1 \Big) \\ & + \frac{1}{2} J_{K_1 K_1} K_1^2 \sigma_1^2 + J_{K_2} \Big(I_2 - \frac{1}{2}\phi_2 \frac{I_2^2}{K_2} - R - \delta_2^k K_2 \Big) + \frac{1}{2} J_{K_2 K_2} K_2^2 \sigma_2^2 + J_{K_1 K_2} K_1 K_2 \sigma_1 \sigma_2 \rho_{12} \\ & + \sum_{i=c,e} \lambda_i(T, \mathbf{X}) \mathbb{E}\big[J(K_1 Z_i, K_2 Z_i, T, \mathbf{X}) - J \big] + \sum_{x \neq \mathbf{X}} \lambda_x(S, T, \mathbf{X}, x) \big[J(K_1, K_2, T, x) - J \big] \Bigg\}, \end{aligned} \tag{A.1}$$

subject to the constraints $D, F_n, G_n, I_n, R \geqslant 0$. Subscripts of J denote partial derivatives, e.g., $J_{K_1} = \frac{\partial J}{\partial K_1}$.

A.2 Optimal Carbon Tax and Negative Emission Technology

The first-order condition for optimal fossil fuel use is

$$f_C(C, J) \Big(\frac{\partial Y_n}{\partial F_n} - b_f \Big) = -J_T \vartheta(\mathbf{X}) \nu_t.$$

Setting the marginal product of fossil fuel equal its marginal cost b_f plus the external costs of emitting greenhouse gases into the atmosphere,

$$\frac{\partial Y_n}{\partial F_n} = b_f + \tau_f.$$

The optimal Pigouvian social cost for using one unit of fossil fuel is thus

$$\tau_f = -\frac{\vartheta(\mathbf{X}) \nu_t J_T C^{1/\psi}}{\delta [(1-\gamma)J]^{1-1/\theta}}.$$

Taking the different units between fossil fuel and carbon emissions into account, the SCC is

$$\tau = -\frac{\vartheta(\mathbf{X}) J_T C^{1/\psi}}{\delta[(1-\gamma)J]^{1-1/\theta}}. \tag{A.2}$$

Since $\varsigma_1 + \varsigma_2 = 1$, the first-order conditions for optimal carbon removal give

$$f_C(C,J)\frac{\partial b_d(S,\mathbf{X},D,K)}{\partial D} = -J_T \vartheta(\mathbf{X}).$$

A.3 Share of Brown Capital

To solve the Hamilton-Jacobi-Bellman equation (A.1), we first transform it by expressing the decision variables in relative terms and reducing the number of state variables by one. Let $g_n = G_n/K_n$, $f_n = F_n/K_n$, $i_n = I_n/K_n$, $r = R/K_1$ denote the relative control variables. Exploiting the homogeneity property of b_d, we use the notation $\widetilde{b}_d(S,\mathbf{X},D) = b_d(S,\mathbf{X},D,K)/K$. We express the value function in terms of total capital $K = K_1 + K_2$ and share of brown capital $S = K_2/(K_1+K_2)$ (instead of K_1 and K_2). Besides, we set $c = C/K$. Using the notation $S_1 = 1-S$, $S_2 = S$, the production functions can then be expressed as

$$Y_n = A_n S_n K \left(\kappa_{1,n} g_n^{\rho_n} + \kappa_{2,n} f_n^{\rho_n}\right)^{\frac{\eta_n}{\rho_n}} \Lambda_n(T).$$

The amounts of consumption goods produced by each sector are

$$C_n = S_n K\Big[A_n\left(\kappa_{1,n} g_n^{\rho_n} + \kappa_{2,n} f_n^{\rho_n}\right)^{\frac{\eta_n}{\rho_n}} \Lambda_n(T,\mathbf{X}) - i_n - b_g(S) g_n - b_f(S) f_n - \frac{\varsigma_n(S)}{S_n}\widetilde{b}_d(S,\mathbf{X},D)\Big].$$

Therefore,

$$\begin{aligned} c = {} & A_1(1-S)\left(\kappa_{1,1} g_1^{\rho_1} + \kappa_{2,1} f_1^{\rho_1}\right)^{\frac{\eta_1}{\rho_1}} \Lambda_1(T,\mathbf{X}) + A_2 S\left(\kappa_{1,2} g_2^{\rho_2} + \kappa_{2,2} f_2^{\rho_2}\right)^{\frac{\eta_2}{\rho_2}} \Lambda_2(T,\mathbf{X}) - i_1(1-S) - i_2 S \\ & - b_g(S)[g_1(1-S) + g_2 S] - b_f(S)[f_1(1-S) + f_2 S] - \widetilde{b}_d(S,\mathbf{X},D). \end{aligned}$$

The dynamics of the state variables can be written as

$$\begin{aligned} \mathrm{d}K_1 &= K_{1-}\Big[\Big(i_1 - \frac{1}{2}\varphi_1 i_1^2 + r - \frac{1}{2}\kappa r^2 - \delta_1^k\Big)\mathrm{d}t + \sigma_1 \mathrm{d}W_1 - \sum_{i=c,e} \ell_i \mathrm{d}N_i\Big], \\ \mathrm{d}K_2 &= K_{2-}\Big[\Big(i_2 - \frac{1}{2}\varphi_2 i_2^2 - r\frac{1-S}{S} - \delta_2^k\Big)\mathrm{d}t + \sigma_2\Big(\rho_{12}\mathrm{d}W_1 + \sqrt{1-\rho_{12}^2}\mathrm{d}W_2\Big) - \sum_{i=c,e} \ell_i \mathrm{d}N_i\Big], \\ \mathrm{d}T &= \widehat{\vartheta}(t,\mathbf{X})[f_1(1-S) + f_2 S]\mathrm{d}t - \vartheta(\mathbf{X}) D\,\mathrm{d}t + \sigma_T \mathrm{d}W_3 + \kappa_{T-}\mathrm{d}X^c, \end{aligned}$$

where $\widehat{\vartheta}(t,\mathbf{X}) = \vartheta(\mathbf{X})K_0 \mathrm{e}^{\int_0^t g_\nu(s)\mathrm{d}s}$. To shorten the notation, we write $W = (W_1, W_2, W_3)^\top$ and denote the drift of the capital stocks and temperature by μ_{K_i} and μ_T, respectively. The dynamics of K and S can be calculated using Ito's lemma:

$$\begin{aligned}
\mathrm{d}S &= S(1-S)\Big[\mu_S(i_1,i_2,r,S)\mathrm{d}t + (\sigma_2\rho_{12} - \sigma_1)\mathrm{d}W_1 + \sigma_2\sqrt{1-\rho_{12}^2}\mathrm{d}W_2\Big], \\
\mathrm{d}K &= K_-\Big[\mu_K(i_1,i_2,r,S)\mathrm{d}t + [(1-S)\sigma_1 + S\sigma_2\rho_{12}]\mathrm{d}W_1 + S\sigma_2\sqrt{1-\rho_{12}^2}\mathrm{d}W_2 - \sum_{i=c,e}\ell_i \mathrm{d}N_i\Big],
\end{aligned}$$

where the drift rates are given by

$$\begin{aligned}
\mu_S(i_1,i_2,r,S) &= \mu_{K_1} - \mu_{K_2} + S(\sigma_1\sigma_2\rho_{12} - \sigma_2^2) + (1-S)(\sigma_1^2 - \sigma_1\sigma_2\rho_{12}), \\
\mu_K(i_1,i_2,r,S) &= (1-S)\mu_{K_1} + S\mu_{K_2}.
\end{aligned}$$

A.4 Separation and Reduced-Form Value Function

We solve a modified HJB equation with finite differences in terms of only three $(S,T,\mathbf{X})$ instead of four state variables $(K_1,K_2,T,\mathbf{X})$. For this to be possible, we must assume that the transition intensities $\lambda_\ell(\mathbf{S},i,j)$ depend on S and T but not explicitly on K_1 and K_2. The following proposition summarizes our findings for the PIGOU state. The situation for the CAP state is discussed in Corollary A.3.

Proposition A.1 (Value Function and Optimal Controls in the PIGOU state)**.** *Let $\widehat{\vartheta}(t,\boldsymbol{X}) = \vartheta(\boldsymbol{X})K_0\mathrm{e}^{\int_0^t g_\nu(s)\mathrm{d}s}$. Suppose that there is no temperature cap in the current state. The value function (2.6) then has the form*

$$J(t,K_1,K_2,T,\boldsymbol{X}) = \frac{1}{1-\gamma}(K_1+K_2)^{1-\gamma}V\big(t,T,S(K_1,K_2),\boldsymbol{X}\big). \tag{A.3}$$

where V satisfies a certain HJB equation which is given in (A.12) below. Optimal consumption is

$$c = \sum_{n=1,2} S_n\Big[A_n\big(\kappa_{1,n}g_n^{\rho_n} + \kappa_{2,n}f_n^{\rho_n}\big)^{\frac{\eta_n}{\rho_n}}\Lambda_n(T,\boldsymbol{X}) - i_n - b_g(S)g_n - b_f(S)f_n - \frac{\varsigma_n}{S_n}\widetilde{b}_d(S,\boldsymbol{X},D)\Big]. \tag{A.4}$$

Optimal energy use is

$$g_1 = \Big(\frac{b_g(S)}{\eta_1 A_1\big(\kappa_{1,1}+\kappa_{2,1}z^{\rho_1}\big)^{\frac{\eta_1}{\rho_1}-1}\Lambda_1(T,\boldsymbol{X})\kappa_{1,1}}\Big)^{\frac{1}{\eta_1-1}}, \qquad f_1 = g_1 z_1, \tag{A.5}$$

$$g_2 = \Big(\frac{b_g(S)}{\eta_2 A_2\big(\kappa_{1,2}+\kappa_{2,2}z^{\rho_2}\big)^{\frac{\eta_2}{\rho_2}-1}\Lambda_2(T,\boldsymbol{X})\kappa_{1,2}}\Big)^{\frac{1}{\eta_2-1}} \qquad f_2 = g_2 z_2, \tag{A.6}$$

where

$$z_1 = \Big(\frac{\kappa_{1,1}}{\kappa_{2,1} b_g(S)}\Big)^{\frac{1}{\rho_1 - 1}} \Big[b_f(S) - \frac{V_T \widehat{\vartheta}(t,\boldsymbol{X})(1-S)}{\big[(1-\gamma)V - V_S S\big][1-\varphi_1 i_1]} \Big]^{\frac{1}{\rho_1 - 1}},$$
$$z_2 = \Big(\frac{\kappa_{1,2}}{\kappa_{2,2} b_g(S)}\Big)^{\frac{1}{\rho_2 - 1}} \Big[b_f(S) - \frac{V_T \widehat{\vartheta}(t,\boldsymbol{X}) S}{\big[(1-\gamma)V - V_S S\big][1-\varphi_1 i_1]} \Big]^{\frac{1}{\rho_2 - 1}}$$

The condition for the optimal reallocation strategy is

$$r = \frac{1}{\kappa}\Big(\frac{V_S}{V_S S + (\gamma - 1)V}\Big) \tag{A.7}$$

and optimal investment and carbon removal solves the nonlinear system

$$\delta(1-\gamma)V^{1-1/\theta} c^{-1/\psi} = \big[(1-\gamma)V - V_S S\big][1-\varphi_1 i_1], \tag{A.8}$$
$$\delta(1-\gamma)V^{1-1/\theta} c^{-1/\psi} = \big[(1-\gamma)V + V_S (1-S)\big][1-\varphi_2 i_2], \tag{A.9}$$
$$\delta(1-\gamma)V^{1-1/\theta} c^{-1/\psi} = -V_T \vartheta(\boldsymbol{X}) \Big(\frac{\partial \widetilde{b}_d(S,\boldsymbol{X},D)}{\partial D}\Big)^{-1}, \tag{A.10}$$

The optimal carbon tax is

$$\tau = \frac{\vartheta(\boldsymbol{X}) c^{1/\psi}}{\delta(\gamma - 1)} \frac{V_T}{V^{1-1/\theta}} K. \tag{A.11}$$

Proof. Let $i_n = I_n/K_n$, $f_n = F_n/K_n$, $g_n = G_n/K_n$, $r = R/K_1$ denote the control variables in relative terms. Substituting these relative controls into (A.1) leads to the HJB equation:

$$\begin{aligned}
0 = \sup_{D, i_n, f_n, g_n, r} \Big\{ & J_t + \frac{\delta}{1 - 1/\psi}[(1-\gamma)J]^{1-1/\theta} \Big(\sum_{n=1,2} [Y_n - I_n - b_g G_n - b_f F_n - \varsigma_n b_d(S,\mathbf{X},D,K)] \Big)^{1-1/\psi} \\
& - \delta\theta J + J_{K_1} K_1 \big(i_1 - \frac{1}{2}\varphi_1 i_1^2 + r - \frac{1}{2}\kappa r^2 - \delta_1^k\big) + J_{K_2} K_2 \big(i_2 - \frac{1}{2}\varphi_2 i_2^2 - r\frac{K_1}{K_2} - \delta_2^k\big) \\
& + \frac{1}{2} J_{K_1 K_1} K_1^2 \sigma_1^2 + \frac{1}{2} J_{K_2 K_2} K_2^2 \sigma_2^2 + J_{K_1 K_2} K_1 K_2 \sigma_1 \sigma_2 \rho_{12} + J_T[\widehat{\vartheta}(f_1 S_1 + f_2 S_2) - \vartheta D] + J_{TT}\frac{1}{2}\sigma_T^2 \\
& + \sum_{i=c,e} \lambda_i(T) \mathbb{E}[J(K_1 Z_i, K_2 Z_i, T, \mathbf{X}) - J] + \sum_{x \neq X} \lambda_x(S,T,\mathbf{X},x)\big[J(K_1,K_2,T,x) - J\big] \Big\}
\end{aligned}$$

We conjecture that the value function has the form

$$J(t,K_1,K_2,T,\mathbf{X}) = \frac{1}{1-\gamma}(K_1 + K_2)^{1-\gamma} V\big(t,T,S(K_1,K_2),\mathbf{X}\big).$$

The partial derivatives of S are $S_{K_1} = -\frac{S}{K}$, $S_{K_2} = \frac{1-S}{K}$. This specification implies[39]

$$V(t,T,S,\mathbf{X}) > 0, \qquad V_T(t,T,S,\mathbf{X}) > 0.$$

The relevant partial derivatives of the value function J are

$$\begin{aligned}
J_{K_1} &= K^{-\gamma}V + \frac{1}{1-\gamma}K^{1-\gamma}V_S\frac{-S}{K},\\
J_{K_1K_1} &= -\gamma K^{-\gamma-1}V + 2K^{-\gamma}V_S\frac{-S}{K} + \frac{1}{1-\gamma}K^{1-\gamma}\Big[V_{SS}\frac{S^2}{K^2} + 2V_S\frac{S}{K^2}\Big],\\
J_{K_2} &= K^{-\gamma}V + \frac{1}{1-\gamma}K^{1-\gamma}V_S\frac{1-S}{K},\\
J_{K_2K_2} &= -\gamma K^{-\gamma-1}V + 2K^{-\gamma}V_S\frac{1-S}{K} + \frac{1}{1-\gamma}K^{1-\gamma}\Big[V_{SS}\frac{(1-S)^2}{K^2} - 2V_S\frac{1-S}{K^2}\Big],\\
J_{K_1K_2} &= -\gamma K^{-1-\gamma}V + K^{-\gamma}V_S\frac{1-2S}{K} + \frac{1}{1-\gamma}K^{1-\gamma}\Big[V_{SS}\frac{-(1-S)S}{K^2} + V_S\frac{2S-1}{K^2}\Big],\\
J_T &= \frac{1}{1-\gamma}K^{1-\gamma}V_T.
\end{aligned}$$

The aggregator is given by $f(C,J) = K^{1-\gamma}\big[\delta\theta V^{1-1/\theta}c^{1-1/\psi} - \delta\theta V\big]$. Substituting the conjecture and its partial derivatives into the HJB equation leads to the following reduced-form HJB equation

$$0 = \sup_{D,f_n,,g_n,i_n,r}\Big\{V_t + M_0 + M_1V + M_2V_S + M_3V_{SS} + M_4V_T + M_5V_{TT}\Big\} \tag{A.12}$$

We introduce the three-dimensional volatility vectors

$$\sigma_k(S) = \big((1-S)\sigma_1 + S\sigma_2\rho_{12}, S\sigma_2\sqrt{1-\rho_{12}^2}, 0\big)^\top, \tag{A.13}$$

$$\sigma_s = \big(\sigma_2\rho_{12} - \sigma_1, \sigma_2\sqrt{1-\rho_{12}^2}, 0\big)^\top. \tag{A.14}$$

The coefficients M_ℓ ($\ell = 1,\dots,5$) are given by

$$\begin{aligned}
M_0 &= \delta\theta V^{1-1/\theta}c^{1-1/\psi} + \sum_{x\neq\mathbf{X}}\lambda_x(S,T,\mathbf{X},x)V(t,T,S,x),\\
M_1 &= (1-\gamma)\Big[\underbrace{(1-S)\mu_1 + S\mu_2}_{=\mu_k} - \frac{1}{2}\gamma[\underbrace{(1-S)^2\sigma_1^2 + S^2\sigma_2^2 + 2S(1-S)\sigma_1\sigma_2\rho_{12}}_{=\|\sigma_k\|^2}]\Big]\\
&\quad + \sum_{i=c,e}\lambda_i(T)\mathbb{E}[(1-\ell_i)^{1-\gamma} - 1] - \sum_{x\neq\mathbf{X}}\lambda_x(S,T,\mathbf{X},x) - \delta\theta,
\end{aligned}$$

[39] The sign of $V_S(t,T,S,\mathbf{X})$ is ambiguous because S indicates how CO_2 intensive the economy is but also how much the economy is diversified, see Hambel et al. (2024) for an extensive discussion about the interaction of abatement and diversification motives.

$$M_2 = S(1-S)\Big(\mu_2 - \mu_1 - \gamma\big[\underbrace{S\sigma_2^2 - (1-S)\sigma_1^2 + (1-2S)\sigma_1\sigma_2\rho_{12}}_{=\sigma_k^\top \sigma_s}\big]\Big),$$

$$M_3 = \frac{1}{2}(1-S)^2 S^2\big[\underbrace{\sigma_1^2 + \sigma_2^2 - 2\sigma_1\sigma_2\rho_{12}}_{=\|\sigma_s\|^2}\big],$$

$$M_4 = \widehat{\vartheta}(t,\mathbf{X})[f_1(1-S) + f_2 S] - \vartheta(\mathbf{X})D,$$

$$M_5 = \frac{1}{2}\sigma_T^2,$$

where c is given in (A.4) and $\widehat{\vartheta}(t,\mathbf{X}) = \vartheta(\mathbf{X})K_0 \mathrm{e}^{\int_0^t g_\nu(s)\mathrm{d}s}$. Calculating the first-order conditions leads to the system of equations (A.5) – (A.9), which determine the optimal controls. The optimal SCC follows from substituting the value function (A.3) into (A.2). □

This proposition is also valid in the BAU state. Policy makers ignore the negative externalities from emitting CO_2, so behave as if $\Lambda_n(T,\mathbf{X}) = 0$ and $\lambda_c(T) = 0$. This implies in particular $V_T = 0$, $D = 0$, and $\tau = 0$.

Corollary A.2 (Tobin's Q's)**.** *Under the conditions of Proposition A.1, the Tobin's Q's of the green and brown asset, respectively, are given by*

$$q_1 = \frac{(1-\gamma)V - V_S S}{\delta(1-\gamma)V^{1-1/\theta}c^{-1/\psi}}, \qquad q_2 = \frac{(1-\gamma)V + V_S(1-S)}{\delta(1-\gamma)V^{1-1/\theta}c^{-1/\psi}}.$$

Proof. This follows immediately from (A.8) and (A.9). □

Now, we consider the case where a temperature cap is implemented in some state $\mathbf{X}$, i.e., carbon emissions are only allowed as long as $T_t \leqslant T_{cap}$. If the carbon budget has been maxed out, i.e. if temperature exceeds T_{cap}, society is not allowed anymore to release CO_2 into the atmosphere.

Corollary A.3 (Optimal Controls in the CAP state)**.** *Suppose that in state $\mathbf{X}$, carbon emissions are prohibited if temperature exceeds its limit T_{cap}.*

(i) If temperature is below the cap, $T \leqslant T_{cap}$, the indirect utility function and the optimal controls are as stated in Proposition A.1.

(ii) If temperature exceeds T_{cap}, the separation (A.3) still holds, but the release of CO_2 into the atmosphere is no longer allowed, i.e. $f_n = 0$. Then, the optimal energy composites are

$$e_n = g_n \kappa_{1,n}^{\frac{1}{\rho_n}} = \begin{cases} \Big[\frac{b_g(S)}{A_n \eta_n \kappa_{1,n}^{\eta_n/\rho_n}\Lambda_n(T)}\Big]^{\frac{1}{\eta_n - 1}} \kappa_{1,n}^{\frac{1}{\rho_n}}, & \text{if } \rho_n > 0 \\ 0, & \text{if } \rho_n \leqslant 0. \end{cases} \tag{A.15}$$

Optimal consumption is

$$c = \sum_{n=1,2} \Big(S_n \Big[A_n e_n^{\eta_n} \Lambda_n(T) - i_n - b_g(S) g_n - \frac{\varsigma_n}{S_n} \widetilde{b}_d(S,\boldsymbol{X},D) \Big] \Big). \tag{A.16}$$

The optimal reallocation strategy is

$$r = \frac{1}{\kappa} \Big(\frac{V_S}{V_S S + (\gamma - 1)V} \Big) \tag{A.17}$$

and optimal investment and optimal carbon removal solve the nonlinear system

$$\delta(1-\gamma) V^{1-1/\theta} c^{-1/\psi} = \big[(1-\gamma)V - V_S S \big] [1 - \varphi_1 i_1], \tag{A.18}$$

$$\delta(1-\gamma) V^{1-1/\theta} c^{-1/\psi} = \big[(1-\gamma)V + V_S (1-S) \big] [1 - \varphi_2 i_2], \tag{A.19}$$

$$\delta(1-\gamma) V^{1-1/\theta} c^{-1/\psi} = -V_T \vartheta(\boldsymbol{X}) \Big(\frac{\partial \widetilde{b}_d(S,\boldsymbol{X},D)}{\partial D} \Big)^{-1}. \tag{A.20}$$

The optimal SCC is as stated in Proposition A.1 and the Tobin's Q's are as stated in Corollary A.2.

Proof. Along the lines of the proof of Proposition A.1. □

Although the decomposition of the indirect utility function and the optimal controls in (i) are unaffected when the temperature cap kicks in, the values are different. This is because V has a different shape in states with and without temperature cap. In the latter scenario, the value function is much steeper as temperature approaches T_{cap}.

A.5 Numerical Solution Approach

Basic Idea We face a problem with an infinite time horizon. To solve this problem we first compute the steady state $\widetilde{V}(T,S,\mathbf{X})$ on a grid $(T,S,\mathbf{X})$ assuming there is no exogenous time trend. Thus, we first have to solve a similar PDE as in (A.12) but without the time derivative. The resulting steady state $\widetilde{V}(T,S,\mathbf{X})$ is then used as a terminal condition $V(t_{\max},T,S,\mathbf{X}) = \widetilde{V}(T,S,\mathbf{X})$ for the value function in the year 2400 corresponding to $t_{\max} = 380$. Starting with this terminal condition, we proceed backwards through the time grid to analyze the transition towards the steady state.

Definition of the Grid We use a grid-based solution approach to solve the non-linear PDE. We discretize the (t,T,S)-space using an equally-spaced lattice. Its grid points are defined by

$$\big\{ (t_n, T_i, S_j) \,|\, n = 0,\cdots,N_t, i = 0,\cdots,N_T, j = 0,\cdots,N_S \big\},$$

where $t_n = n\Delta_t$, $T_i = i\Delta_T$, and $S_j = j\Delta_S$ for some fixed grid size parameters Δ_t, Δ_T, and Δ_S that denote the distances between two grid points. The numerical results are based on a choice of $N_T = 50$, $N_S = 200$ and one time step per year. Our results hardly change if we use a finer grid or more time steps per year. In the sequel, $V_{n,i,j,k}$ denotes the approximated value function at the grid point $(t_n, T_i, S_j, \mathbf{X} = k)$ and $\pi_{n,i,j,k}$ refers to the corresponding set of optimal controls. We apply an implicit finite-difference scheme.

Finite Differences Approach We now describe the numerical solution approach in more detail. We adapt the numerical solution approach used by Munk and Sørensen (2010). The numerical procedure works as follows. At any point in time, we make a conjecture for the optimal strategy $\pi^*_{n,i,j,k}$. A good guess is the value at the previous grid point since the abatement strategy varies only slightly over a small time interval, i.e. we set $\pi_{n-1,i,j,k} = \pi^*_{n,i,j,k}$. Substituting this guess into the HJB equation yields a semi-linear PDE:

$$0 = V_t + \delta\theta V^{1-1/\theta} c^{1-1/\psi} + \sum_{x \neq \mathbf{X}} \lambda_x(S,T,\mathbf{X},x) V(t,T,S,x) + M_1 V + M_2 V_T + M_3 V_{TT} + M_4 V_S + M_5 V_{SS}$$

with state-dependent coefficients $M_i = M_i(t,T,S,\mathbf{X})$ as stated in Appendix A.4. Due to the implicit approach, we approximate the time derivative by forward finite differences. In the approximation, we use the so-called *up-wind* scheme that stabilizes the finite differences approach. Therefore, the relevant finite differences at the grid point (n,i,j,k) are given by

$$\begin{aligned}
\mathrm{D}_T^+ V_{n,i,j,k} &= \frac{V_{n,i+1,j,k} - V_{n,i,j,k}}{\Delta_T}, & \mathrm{D}_T^- V_{n,i,j,k} &= \frac{V_{n,i,j,k} - V_{n,i-1,j,k}}{\Delta_T}, \\
\mathrm{D}_S^+ V_{n,i,j,k} &= \frac{V_{n,i,j+1,k} - V_{n,i,j,k}}{\Delta_S}, & \mathrm{D}_S^- V_{n,i,j,k} &= \frac{V_{n,i,j,k} - V_{n,i,j-1,k}}{\Delta_S}, \\
\mathrm{D}_{TT}^2 V_{n,i,j,k} &= \frac{V_{n,i+1,j,k} - 2V_{n,i,j,k} + V_{n,i-1,j,k}}{\Delta_T^2}, \\
\mathrm{D}_{SS}^2 V_{n,i,j,k} &= \frac{V_{n,i,j+1,k} - 2V_{n,i,j,k} + V_{n,i,j-1,k}}{\Delta_S^2}, \\
\mathrm{D}_t^+ V_{n,i,j,k} &= \frac{V_{n+1,i,j,k} - V_{n,i,j,k}}{\Delta_t}.
\end{aligned}$$

Substituting these expressions into the PDE above yields the following semi-linear equation for the grid point (t_n, T_i, S_j, k):

$$\begin{aligned}
V_{n+1,i,j,k} \frac{1}{\Delta_t} = V_{n,i,j,k} \Big[-M_1 + \frac{1}{\Delta_t} + \mathrm{abs}\Big(\frac{M_2}{\Delta_T}\Big) + \mathrm{abs}\Big(\frac{M_4}{\Delta_S}\Big) + 2\frac{M_3}{\Delta_T^2} + 2\frac{M_5}{\Delta_S^2} \Big] \\
+ V_{n,i-1,j,k} \Big[\frac{M_2^-}{\Delta_T} - \frac{M_3}{\Delta_T^2} \Big] + V_{n,i+1,j,k} \Big[-\frac{M_2^+}{\Delta_T} - \frac{M_3}{\Delta_T^2} \Big]
\end{aligned}$$

$$+V_{n,i,j-1,k}\Big[\frac{M_4^-}{\Delta_S}-\frac{M_5}{\Delta_S^2}\Big]+V_{n,i,j+1,k}\Big[-\frac{M_4^+}{\Delta_S}-\frac{M_5}{\Delta_S^2}\Big]$$
$$+\delta\theta V_{n,i,j,k}^{1-1/\theta}c_{n,i,j,k}^{1-1/\psi}+\sum_{\widehat{k}\neq k}\lambda(S,T,k,\widehat{k})V_{n,i,j,\widehat{k}}.$$

Therefore, for a fixed point in time each grid point is determined by a non-linear equation. This results in a non-linear system of $(N_S+1)(N_T+1)$ equations for every state k of the Markov chain $\mathbf{X}$ that can be solved for the vector

$$V_{n,k}=(V_{n,1,1,k},\cdots,V_{n,1,N_S,k},V_{n,2,1,k},\cdots,V_{n,2,N_S,k},\cdots,V_{n,N_T,1,k},\cdots,V_{n,N_T,N_S,k}).$$

Using this solution we update our conjecture for the optimal controls at the current point in the time dimension. We apply the first-order conditions as stated in Proposition A.1 and determine the optimal strategies and the optimal SCC with the above-mentioned finite-difference approximations of the corresponding partial derivatives. After we have solved the model, we simulate all state and decision variables in a Monte-Carlo simulation. We simulate 200,000 paths and calculate quantiles, means, and other moments for all relevant variables.

B Asset Pricing

B.1 Dynamics of the Stochastic Discount Factor

Duffie and Epstein (1992a) show that the dynamics of the pricing kernel H are given by

$$\frac{\mathrm{d}H}{H_-}=\frac{\mathrm{d}f_c(C,J)}{f_c(C,J)}+f_J(C,J)\mathrm{d}t.$$

The relevant partial derivatives of the aggregator are

$$f_c(C,J)=\delta V^{1-1/\theta}K^{-\gamma}c^{-1/\psi},\qquad f_J(C,J)=\delta(\theta-1)c^{1-1/\psi}V^{-1/\theta}-\delta\theta.$$

To calculate the dynamics of the SDF, we first compute

$$\frac{\mathrm{d}K^{-\gamma}}{K_-^{-\gamma}}=\Big(-\gamma\mu_k+\frac{1}{2}\gamma(\gamma+1)\|\sigma_k\|^2\Big)\mathrm{d}t-\gamma\sigma_k^\top\mathrm{d}W+\sum_{i=c,e}\big((1-\ell_i)^{-\gamma}-1\big)\mathrm{d}N_i.$$

Secondly, we determine the dynamics of $V^{1-1/\theta}$. According to Ito's lemma, $V=V(t,S,T,\mathbf{X})$ satisfies

$$\frac{\mathrm{d}V}{V_-}=\mu_v\mathrm{d}t+\sigma_v^\top\mathrm{d}W-\sum_{x\neq\mathbf{X}}j_v^x\mathrm{d}N^x$$

where N^x is a point process that indicates a jump to state x, i.e.,

$$N^x_{\tau_x} = \begin{cases} N^x_{\tau_x-} + 1 : & \mathbf{X}_{\tau_x} = x, \mathbf{X}_{\tau_x-} \neq x \\ N^x_{\tau_x-} : & \text{else} \end{cases}$$

with

$$\begin{aligned} \mu_v = \frac{1}{V_-}\Big(& V_t + V_S S(1-S)\mu_s + V_T \vartheta \nu (f_1(1-S) + f_2 S) - V_T \vartheta D \\ & + \frac{1}{2} V_{SS} S^2 (1-S)^2 \|\sigma_s\|^2 + \frac{1}{2} V_{TT} \sigma_T^2 \Big), \end{aligned} \tag{B.1}$$

$$\sigma_v = \frac{1}{V_-}\Big(V_S S(1-S)(-\sigma_1 + \sigma_2 \rho_{12}),\, V_S S(1-S)\sigma_2 \sqrt{1-\rho_{12}^2},\, V_T \sigma_T \Big)^\top, \tag{B.2}$$

$$j_v^x = 1 - \frac{V(t,T,S,x)}{V(t,T,S,\mathbf{X})}. \tag{B.3}$$

Another application of Ito's lemma yields

$$\frac{\mathrm{d}V^{1-1/\theta}}{V_-^{1-1/\theta}} = \Big[\frac{\theta-1}{\theta}\mu_v - \frac{\theta-1}{2\theta^2}\|\sigma_v\|^2 \Big]\mathrm{d}t + \frac{\theta-1}{\theta}\sigma_v^\top \mathrm{d}W + \sum_{x \neq \mathbf{X}} \big((1-j_v^x)^{1-1/\theta} - 1 \big)\mathrm{d}N^x.$$

Therefore, by Ito's product rule,

$$\begin{aligned} \frac{\mathrm{d}(V^{1-1/\theta}K^{-\gamma})}{(V^{1-1/\theta}K^{-\gamma})_-} = & \Big(-\gamma\mu_k + \frac{1}{2}\gamma(\gamma+1)\|\sigma_k\|^2 \Big)\mathrm{d}t + \frac{\theta-1}{\theta}\Big(\mu_v - \gamma\langle \sigma_k, \sigma_s \rangle \frac{V_S}{V} S(1-S) \Big)\mathrm{d}t \\ & - \frac{\theta-1}{2\theta^2}\|\sigma_s\|^2 \frac{V_S^2}{V^2} S^2 (1-S)^2 \mathrm{d}t + \Big(\frac{\theta-1}{\theta}\sigma_v - \gamma\sigma_k \Big)^\top \mathrm{d}W + \sum_{i=c,e} \big((1-\ell_i)^{-\gamma} - 1 \big)\mathrm{d}N_i \\ & + \sum_{x \neq \mathbf{X}} \big((1-j_v^x)^{1-1/\theta} - 1 \big)\mathrm{d}N^x. \end{aligned} \tag{B.4}$$

Notice that according to the simplified HJB equation (A.12),

$$\begin{aligned} \mu_v - \gamma\langle \sigma_k, \sigma_s \rangle \frac{V_S}{V} S(1-S) = & (\gamma-1)\big(\mu_k - \frac{1}{2}\gamma\|\sigma_k\|^2 \big) + \delta\theta - \delta\theta V^{-1/\theta} c^{1-1/\psi} \\ & - \sum_{i=c,e} \lambda_i \mathbb{E}[(1-\ell_i)^{1-\gamma} - 1] + \sum_{x \neq \mathbf{X}} \lambda_x j_v^x, \end{aligned}$$

where we use the short-hand notation $\lambda_x = \lambda_x(\mathbf{S}, \mathbf{X}, x)$. Substituting this term into (B.4) yields

$$\begin{aligned} \frac{\mathrm{d}(V^{1-1/\theta}K^{-\gamma})}{(V^{1-1/\theta}K^{-\gamma})_-} = & \Big(-\gamma\mu_k + \frac{1}{2}\gamma(\gamma+1)\|\sigma_k\|^2 \Big)\mathrm{d}t - \frac{\theta-1}{2\theta^2}\|\sigma_s\|^2 \frac{V_S^2}{V^2} S^2 (1-S)^2 \mathrm{d}t \\ & + \Big(\frac{\theta-1}{\theta}\sigma_v - \gamma\sigma_k \Big)^\top \mathrm{d}W \end{aligned}$$

$$+\frac{\theta-1}{\theta}\Big((\gamma-1)\big(\mu_k-\frac{1}{2}\gamma\|\sigma_k\|^2\big)+\delta\theta-\delta\theta V^{-1/\theta}c^{1-1/\psi}\Big)\mathrm{d}t+\sum_{i=c,e}\big((1-\ell_i)^{-\gamma}-1\big)\mathrm{d}N_i$$
$$+\sum_{x\neq\mathbf{X}}\big((1-j_v^x)^{1-1/\theta}-1\big)\mathrm{d}N^x-\frac{\theta-1}{\theta}\Big(\sum_{i=c,e}\lambda_i\mathbb{E}[(1-\ell_i)^{1-\gamma}-1]-\sum_{x\neq\mathbf{X}}\lambda_x j_v^x\Big)\mathrm{d}t.$$

Furthermore, the consumption-capital ratio $c=C/K$ has the following dynamics

$$\frac{\mathrm{d}c}{c_-}=\mu_c\mathrm{d}t+\sigma_c^\top\mathrm{d}W-\sum_{x\neq\mathbf{X}}j_c^x\mathrm{d}N^x$$

for auxiliary functions $\mu_c(t,T,S,\mathbf{X})$ and $\sigma_c(t,T,S,\mathbf{X})$, which can be determined numerically, and

$$j_c^x=1-\frac{c(t,T,S,x)}{c(t,T,S,\mathbf{X})}. \tag{B.5}$$

In turn,

$$\frac{\mathrm{d}c^{-1/\psi}}{c_-^{-1/\psi}}=-\frac{1}{\psi}(\mu_c\mathrm{d}t+\sigma_c^\top\mathrm{d}W)+\frac{1+\psi}{\psi^2}\|\sigma_c\|^2\mathrm{d}t+\sum_{x\neq\mathbf{X}}\big((1-j_c^x)^{-1/\psi}-1\big)\mathrm{d}N^x$$

Consequently, the pricing kernel dynamics are given by

$$\begin{aligned}\frac{\mathrm{d}H_-}{H_-}=&-r_t^f\mathrm{d}t+\Big(-\gamma\sigma_k+\frac{\theta-1}{\theta}\sigma_v-\frac{1}{\psi}\sigma_c\Big)^\top\mathrm{d}W+\sum_{i=c,e}\big((1-\ell_i)^{-\gamma}-1\big)\mathrm{d}N_i-\lambda_i\mathbb{E}[(1-\ell_i)^{-\gamma}-1]\mathrm{d}t\\&+\sum_{x\neq\mathbf{X}}\Big[\big((1-j_v^x)^{1-1/\theta}(1-j_c^x)^{-1/\psi}-1\big)\mathrm{d}N^x-\lambda_x\big((1-j_v^x)^{1-1/\theta}(1-j_c^x)^{-1/\psi}-1\big)\mathrm{d}t\Big],\end{aligned} \tag{B.6}$$

where the risk-free rate is given by

$$\begin{aligned}r_t^f=&\,\delta+\frac{1}{\psi}\mu_k-\frac{1}{2}\gamma\Big(1+\frac{1}{\psi}\Big)\|\sigma_k\|^2-\Big(\frac{1+\psi}{\psi^2}\|\sigma_c\|^2-\frac{\theta-1}{2\theta^2}\|\sigma_v\|^2-\frac{1}{\psi}\sigma_c^\top\Big(\frac{\theta-1}{\theta}\sigma_v-\gamma\sigma_k\Big)\Big)\\&-\sum_{i=c,e}\lambda_i\mathbb{E}\Big[(1-\ell_i)^{-\gamma}-1+\frac{\psi^{-1}-\gamma}{1-\gamma}\big(1-(1-\ell_i)^{1-\gamma}\big)\Big]\\&-\sum_{x\neq\mathbf{X}}\Big[\lambda_x\big((1-j_v^x)^{1-1/\theta}(1-j_c^x)^{-1/\psi}-1\big)+\frac{\theta-1}{\theta}\lambda_x j_v^x\Big].\end{aligned} \tag{B.7}$$

An application of Itô's lemma gives the drift and volatility vector of optimal consumption as

$$\mu_C(t,T,S)=\mu_k(S)+\mu_c(t,T,S)+\sigma_c(t,T,S)^\top\sigma_k(S), \tag{B.8}$$
$$\sigma_C(t,T,S)=\sigma_k(S)+\sigma_c(t,T,S). \tag{B.9}$$

Substituting (B.8) and (B.9) into the pricing kernel dynamics and some algebra completes the proof. □

B.2 Dividend Dynamics

The amount of consumption goods produced by asset n are

$$C_n = Y_n - I_n - b_f F_n - b_g G_n - b_d(S,\mathbf{X},D,K) = \chi_n K_n$$

with $\chi_n = \left[A_n\left(\kappa_{1,n} g_n^{\rho_n} + \kappa_{2,n} f_n^{\rho_n}\right)^{\frac{\eta_n}{\rho_n}} \Lambda_n(T) - i_n - b_g(S) g_n - b_f(S) f_n - \widetilde{b}_d(S,\mathbf{X},D)\right]$. An application of Ito's lemma shows that χ_n evolves according to

$$\frac{\mathrm{d}\chi_n}{\chi_{n-}} = \mu_{\chi_n}\mathrm{d}t + \sigma_{\chi_n}^\top \mathrm{d}W - \sum_{x\neq\mathbf{X}} j_{\chi_n}^x \mathrm{d}N^x$$

for auxiliary functions μ_{χ_n}, σ_{χ_n}, $j_{\chi_n}^x$ that can be determined numerically along the lines of (B.1) – (B.3). Notice that χ_n is unaffected when the economy is hit by an economic Barro-type disaster shock N^d.

Empirically, dividends are more volatile than consumption (e.g. Bansal and Yaron 2004) and dividends fall more than consumption when a disaster hits the economy (e.g. Longstaff and Piazzesi 2004). Following Wachter (2013), among others, we thus model dividends as levered consumption, i.e. $\mathscr{D}_n = C_n^\phi$ for $\phi \geqslant 1$.[40] An application of Ito's product rule yields the dividend dynamics

$$\frac{\mathrm{d}\mathscr{D}_n}{\mathscr{D}_{n-}} = \mu_{\mathscr{D}_n}\mathrm{d}t + \sigma_{\mathscr{D}_n}^\top \mathrm{d}W + \sum_{i=c,e} j_{\mathscr{D}_n}^i \mathrm{d}N^i + \sum_{x\neq\mathbf{X}} j_{\mathscr{D}_n}^x \mathrm{d}N^x$$

with

$$\begin{aligned}
\mu_{\mathscr{D}_n} &= \phi(\mu_{K_n} + \mu_{\chi_n} + \sigma_{\chi_n}^\top \sigma_{K_n}) + \frac{1}{2}\phi(\phi-1)\|\sigma_{K_n} + \sigma_{\chi_n}\|^2,\\
\sigma_{\mathscr{D}_n} &= \phi(\sigma_{K_n} + \sigma_{\chi_n}),\\
j_{\mathscr{D}_n}^i &= (1-\ell_i)^\phi - 1,\\
j_{\mathscr{D}_n}^x &= (1-j_{\chi_n}^x)^\phi - 1.
\end{aligned}$$

In a next step, we determine the dynamics of discounted dividends, $\widehat{\mathscr{D}}_n = H\mathscr{D}_n$. Another application of Itô's product rule implies

$$\frac{\mathrm{d}\widehat{\mathscr{D}}_n}{\widehat{\mathscr{D}}_{n-}} = \mu_{\widehat{\mathscr{D}}_n}\mathrm{d}t + \sigma_{\widehat{\mathscr{D}}_n}^\top \mathrm{d}W + \sum_{i=c,e} j_{\widehat{\mathscr{D}}_n}^i \mathrm{d}N_i + \sum_{x\neq\mathbf{X}} j_{\widehat{\mathscr{D}}_n}^x \mathrm{d}N^x$$

[40] A popular alternative to this approach is modelling the consumption-dividend ratio as a stationary but persistent process, as in Longstaff and Piazzesi (2004), among others. In order to focus on the novel implications of climate transition risk on asset prices, we keep the setting simple although following this approach would also be feasible in our setting.

with

$$\begin{aligned}
\mu_{\widehat{\mathscr{D}}_n} &= \mu_H + \mu_{\mathscr{D}_n} + \sigma_H^\top \sigma_{D_n}, \\
\sigma_{\widehat{\mathscr{D}}_n} &= \sigma_H + \sigma_{\mathscr{D}_n}, \\
j^i_{\widehat{\mathscr{D}}_n} &= (1-\ell_i)^{\phi-\gamma} - 1, \\
j^x_{\widehat{\mathscr{D}}_n} &= (1-j^x_{\chi_n})^{\phi}(1-j^x_v)^{1-1/\theta}(1-j^x_c)^{-1/\psi} - 1.
\end{aligned}$$

B.3 Price-dividend Ratios of Dividend Claims

Let $\Pi_n = \frac{P_n}{\mathscr{D}_n}$ denote the price-dividend ration of asset n, and $\pi_n = \log\left(\frac{P_n}{\mathscr{D}_n}\right)$ the log price-dividend ratio. Due to the representation of the dividends, the dynamics of K_n, and the pricing equation, the price is linear in K_n and thus the price-dividend ratio is independent of K_n. Therefore, it is not driven by the disaster risk process N^d, and the dynamics of the log price-dividend ratio can be written as

$$\frac{\mathrm{d}\pi_n}{\pi_{n-}} = \mu_{\pi_n}\mathrm{d}t + \sigma_{\pi_n}^\top \mathrm{d}W - \sum_{x\neq \mathbf{X}} j^x_{\pi_n}\mathrm{d}N^x,$$

where the drift and the volatility vector are given by

$$\begin{aligned}
\mu_{\pi_n} &= \frac{1}{\pi_n}\Big[\pi_{n,t} + \pi_{n,S}S(1-S)\mu_S + \pi_{n,T}\mu_T + \frac{1}{2}\pi_{n,TT}\|\sigma_T\|^2 + \frac{1}{2}\pi_{n,SS}S^2(1-S)^2\|\sigma_S\|^2\Big], \\
\sigma_{\pi_n} &= \frac{1}{\pi_n}\Big[\pi_{n,T}\sigma_T + \pi_{n,S}S(1-S)\sigma_S\Big], \\
j^x_{\pi_n} &= 1 - \frac{\pi_n(t,T,S,x)}{\pi_n(t,T,S,\mathbf{X})}.
\end{aligned}$$

In particular, the price-dividend ratio $\Pi_n = \mathrm{e}^{\pi_n}$ satisfies the following dynamics

$$\frac{\mathrm{d}\Pi_n}{\Pi_{n-}} = \big(\pi_n\mu_{\pi_n} + \frac{1}{2}\pi_n^2\|\sigma_{\pi_n}\|^2\big)\mathrm{d}t + \pi_n\sigma_{\pi_n}^\top \mathrm{d}W - \sum_{x\neq\mathbf{X}} j^x_{\Pi_n}\mathrm{d}N^x,$$

where

$$j^x_{\Pi_n} = 1 - \frac{\Pi_n(t,T,S,x)}{\Pi_n(t,T,S,\mathbf{X})}.$$

We rewrite the discounted asset price HP_n as $\widehat{P}_n(\widehat{\mathscr{D}}_n,\pi_n) = \widehat{\mathscr{D}}_n\mathrm{e}^{\pi_n}$. An application of Itô's lemma implies

$$\frac{\mathrm{d}\widehat{P}_n}{\widehat{P}_{n-}} = \big(\mu_{\widehat{\mathscr{D}}_n} + \pi_n\mu_{\pi_n} + \frac{1}{2}\pi_n^2\|\sigma_{\pi_n}\|^2 + \pi_n\sigma_{\pi_n}^\top\sigma_{\widehat{\mathscr{D}}_n}\big)\mathrm{d}t + (\pi_n\sigma_{\pi_n} + \sigma_{\widehat{\mathscr{D}}_n})^\top \mathrm{d}W$$

$$+\sum_{i=c,e}\big((1-\ell_i)^{\phi-\gamma}-1\big)\mathrm{d}N_i+\sum_{x\neq\mathbf{X}}\big((1-j^x_{\Pi_n})(1+j^x_{\widehat{\mathscr{D}}_n})-1\big)\mathrm{d}N^x.$$

An application of the Feynman-Kač Theorem yields

$$\mathscr{L}\widehat{P}_n+\mathrm{e}^{-\pi_n}\widehat{P}_n=0, \tag{B.10}$$

where $\mathscr{L}\widehat{P}_n$ denotes the infinitesimal generator. The no-arbitrage condition implies

$$\begin{aligned}\frac{\mathscr{L}\widehat{P}_n}{\widehat{P}_{n-}}&=\mu_{\widehat{\mathscr{D}}_n}+\pi_n\mu_{\pi_n}+\frac{1}{2}\pi_n^2\|\sigma_{\pi_n}\|^2+\pi_n\sigma_{\pi_n}^\top\sigma_{\widehat{\mathscr{D}}_n}+\sum_{i=c,e}\lambda_i(T)\mathbb{E}\big[(1-\ell_i)^{\phi-\gamma}-1\big]\\&\quad+\sum_{x\neq\mathbf{X}}\lambda_x\big((1-j^x_{\Pi_n})(1+j^x_{\widehat{\mathscr{D}}_n})-1\big).\end{aligned} \tag{B.11}$$

Substituting (B.11) into (B.10) yields

$$\begin{aligned}0&=\mu_{\widehat{\mathscr{D}}_n}+\pi_n\mu_{\pi_n}+\frac{1}{2}\pi_n^2\|\sigma_{\pi_n}\|^2+\pi_n\sigma_{\pi_n}^\top\sigma_{\widehat{\mathscr{D}}_n}+\sum_{i=c,e}\lambda_i(T)\mathbb{E}\big[(1-\ell_i)^{\phi-\gamma}-1\big]+\mathrm{e}^{-\pi_n}\\&\quad+\sum_{x\neq\mathbf{X}}\lambda_x\big((1-j^x_{\Pi_n})(1+j^x_{\widehat{\mathscr{D}}_n})-1\big).\end{aligned}$$

Consequently, we obtain the following partial differential equation for the log price-dividend ratio π_n:

$$\begin{aligned}0&=\mathrm{e}^{-\pi_n}+\mu_{\widehat{\mathscr{D}}_n}+\pi_{n,t}+\pi_{n,S}S(1-S)\mu_S+\pi_{n,T}\mu_T+\frac{1}{2}(\pi_{n,TT}+\pi_{n,T}^2)\|\sigma_T\|^2\\&\quad+\frac{1}{2}(\pi_{n,SS}+\pi_{n,S}^2)S^2(1-S)^2\|\sigma_S\|^2+\big(\pi_{n,T}\sigma_T+\pi_{n,S}S(1-S)\sigma_S\big)^\top\sigma_{\widehat{\mathscr{D}}_n}\\&\quad+\sum_{i=c,e}\lambda_i(T)\mathbb{E}\big[(1-\ell_i)^{\phi-\gamma}-1\big]+\sum_{x\neq\mathbf{X}}\lambda_x\big((1-j^x_{\Pi_n})(1+j^x_{\widehat{\mathscr{D}}_n})-1\big).\end{aligned}$$

Notice that this PDE is nonlinear since it involves squared partial derivatives of π_n. To simplify the numerical solution approach, we transform this PDE into a linear, parabolic PDE that can be solved using finite differences. We substitute $\Pi_n=\mathrm{e}^{\pi_n}$ and end up with

$$\begin{aligned}0&=1+\sum_{x\neq\mathbf{X}}\lambda_x\Pi_n(t,T,S,x)(1+j^x_{\widehat{\mathscr{D}}_n})+\Pi_n\Big(\mu_{\widehat{\mathscr{D}}_n}+\sum_{i=c,e}\lambda_i(T)\mathbb{E}\big[(1-\ell_i)^{\phi-\gamma}-1\big]-\sum_{x\neq\mathbf{X}}\lambda_x\Big)\\&\quad+\Pi_{n,t}+\Pi_{n,S}S(1-S)\mu_S+\Pi_{n,T}\mu_T+\frac{1}{2}\Pi_{n,TT}\|\sigma_T\|^2+\frac{1}{2}\Pi_{n,SS}S^2(1-S)^2\|\sigma_S\|^2\\&\quad+\big(\Pi_{n,T}\sigma_T+\Pi_{n,S}S(1-S)\sigma_S\big)^\top\sigma_{\widehat{\mathscr{D}}_n}\end{aligned} \tag{B.12}$$

B.4 Risk Premiums

The dynamics of the asset price $P_n = \mathrm{e}^{\pi_n}\mathscr{D}_n$ follow by Itô's lemma. We obtain the following asset price dynamics

$$\begin{aligned}\frac{\mathrm{d}P_n}{P_{n-}} = \mu_n^p \mathrm{d}t + (\sigma_{\pi_n} + \sigma_{\mathscr{D}_n})^\top \mathrm{d}W + \sum_{i=c,e} \big((1-\ell_i)^\phi - 1\big)\mathrm{d}N_i - \lambda_i(T)\mathbb{E}\big[(1-\ell_i)^\phi - 1\big]\mathrm{d}t \\ + \sum_{x\neq \mathbf{X}} \Big[\big((1-j^x_{\Pi_n})(1-j^x_{\chi_n})^\phi - 1\big)\mathrm{d}N^x - \lambda_x\big((1-j^x_{\Pi_n})(1-j^x_{\chi_n})^\phi - 1\big)\Big],\end{aligned}$$

where the expected stock return and the volatility vector are given by

$$\mu_n^p = \mu_{\pi_n} + \mu_{\mathscr{D}_n} + \sigma_{\mathscr{D}_n}^\top \sigma_{\pi_n} + \frac{1}{2}\|\sigma_{\pi_n}\|^2 + \sum_{i=c,e} \lambda_i(T)\mathbb{E}\big[(1-\ell_i)^\phi - 1\big] + \sum_{x\neq \mathbf{X}} \lambda_x\big((1-j^x_{\Pi_n})(1+j^x_{\mathscr{D}_n}) - 1\big).$$

Now, the risk premium of asset n can be computed as the sum of its expected stock return, μ_n^P, and its dividend yield, $y_n^d = \mathrm{e}^{-\pi_n}$, minus the risk-free interest rate, r^f, i.e.

$$r_n^p = \mu_n^p + y_n^d - r^f.$$

To derive a semi-closed form solution of the equity premium and the carbon premium, we multiply risk exposures with the appropriate market prices of risk and obtain

$$\begin{aligned}r_n^p = \big(\Pi_{n,T}\sigma_T + \Pi_{n,S}S(1-S)\sigma_S + \phi\sigma_n + \phi\sigma_{\chi_n}\big)^\top \Big(\gamma\sigma_k - \frac{\theta-1}{\theta}\sigma_v + \frac{1}{\psi}\sigma_c\Big) \\ + \sum_{i=c,e} \lambda_i(T)\mathbb{E}\big[\big(1-(1-\ell_i)\big)^{-\gamma}\big((1-\ell_i)^\phi - 1\big)\big] \\ + \sum_{x\neq \mathbf{X}} \lambda_x\big(1-(1-j_v^x)^{1-1/\theta}(1-j_c^x)^{-1/\psi}\big)\big((1-j^x_{\Pi_n})(1+j^x_{\chi_n}) - 1\big).\end{aligned} \tag{B.13}$$

The decomposition (B.13) of the equity premium generalizes formulas similar to this as in van den Bremer et al. (2023) and Karydas and Xepapadeas (2022) to transition risk. It is known from the disaster risk literature that the disaster risk component in the second line typically makes the largest contribution to the equity premium while the diffusion component in the first line has only a small effect.

The novel component is the transition risk term in the third line. The first factor $\big(1-(1-j_v^x)^{1-1/\theta}(1-j_c^x)^{-1/\psi}\big)$ reflects the effect of a transition shock on the stochastic discount factor and is similar to the corresponding term in the risk-free rate. The second factor $\big((1-j^x_{\Pi_n})(1+j^x_{\chi_n})-1\big)$ reflects the impact of transition shock on the share price of sector n. If this price impact is positive, the last term contributes positively to the risk premium. Moreover, if the price impact of a certain type of shock is more pro-

nounced for the brown sector, then a carbon premium emerges. However, the carbon premium can also emerge from diffusive components as can be seen from the first line: In the CAP state, a temperature shock with volatility σ_T can have very distinct effects on the green and the brown sector if temperatures are close to two degrees, and thus the difference between $\Pi_{2,T}$ and $\Pi_{1,T}$ can drive to the carbon premium.

C Details on the Calibration

Here we provide further calibration details for all relevant parts of the core and extended models. We also present alternative calibrations used for sensitivity analyses and robustness checks.

C.1 Calibration of the Core Model

Our calibration is matched to the global economy[41] and is market-based. For the political Markov chain, we assume a constant probability of 4% that there is a switch from BAU to active climate policy, and a zero probability that there is a switch back to no carbon pricing again.

Macroeconomic Uncertainty We set annual volatility of capital diffusion risk to $\sigma_1 = \sigma_2 = 2\%$ matching the observed volatility of consumption or output (e.g., Wachter 2013). We assume a zero *instantaneous correlation* between the two capital stocks, $\rho_{12} = 0$ (cf. Cochrane et al., 2007). The total correlation between capital stocks is much higher than indicated by the value of ρ_{12} due to joint macroeconomic disaster shocks and common state variables that affect both sectors (cf. Hambel et al., 2024).

The recovery rate of macroeconomic disasters, $Z = 1 - \ell$, has a power distribution over $(0,1)$ with parameter $\alpha > 0$ and density functions $\zeta(Z) = \alpha Z^{\alpha-1}$, $Z \in (0,1)$ (Pindyck and Wang, 2013). The n^{th} moment of the recovery rate is $\mathbb{E}[Z^n] = \frac{\alpha}{\alpha+n}$. To calibrate the macroeconomic disaster-size distribution, we follow Wachter (2013) and define a disaster as an event destroying more than $\overline{\ell} = 10\%$ of GDP or aggregate consumption. She uses historical consumption data to estimate an annual disaster probability of 3.55% and an average consumption loss of 25% when a disaster strikes: $\lambda \int_0^{1-\overline{\ell}} \zeta(Z) \mathrm{d}Z = 0.0355$ and $\mathbb{E}[\ell | \ell > \overline{\ell}] = 0.25$. This pins down $\alpha = 5$ and $\lambda = 0.06$.

Economic Growth To jointly calibrate the production and preference parameters, we follow Hambel et al. (2024) and firstly consider a model with only one capital share in the spirit of Pindyck and Wang

[41] This is true for consumption, GDP, and capital stocks, but for lack of better data and following Pindyck and Wang (2013) we calibrate the returns on safe and risky assets to U.S. data.

(2013). Their model also abstracts from climate change, but it is nested in our two-sector model. The model is well-suited to explain *historical* asset returns, since dirty capital dominated the world economy in the past, while the influence of climate change on asset markets was modest. We assume that the single-capital stock evolves according to

$$\mathrm{d}K = \left(I - \frac{1}{2}\varphi\frac{I^2}{K} - \delta_k K\right)\mathrm{d}t + K\sigma\mathrm{d}W - K_-\ell_e\mathrm{d}N_e.$$

Besides, output is produced by capital K and energy E by a Cobb-Douglas production technology, $Y = AK^{1-\eta}E^{\eta} = I + C + bE$, where b is the price of one unit of the energy composite E. In the optimum, the model becomes a simple AK-technology with linear production function $Y = A^*K$ where productivity is

$$A^* = A\left(\frac{b}{\eta A}\right)^{\frac{\eta}{\eta-1}}.$$

This aggregate model closely follows Pindyck and Wang (2013), but involves an energy input E. We solve this model for a representative investor with Epstein-Zin-preferences and obtain a set of non-linear equations that pin down the model parameters.

Fixing the leverage parameter at $\phi = 2.6$ (Wachter 2013) and the elasticity of intertemporal subsitution at $\psi = 1.5$ (Bansal and Yaron 2004), we calibrate the remaining parameters to match an expected GDP growth rate of $\overline{\mu} = 2.52\%$ in normal times, i.e. in the absence of a disaster (Wachter 2013), an average consumption rate of $\frac{C}{Y} = 63\%$ of GDP, a risk-free interest rate of $r^f = 0.8\%$, an equity premium of $r^p = 6.6\%$, and a Tobin's Q of 1.548 (Pindyck and Wang 2013).

All real quantities (emissions, GDP, capital stocks, etc.) are calibrated to the global economy, but we follow Pindyck and Wang (2013) and take the safe rate to be the return on U.S. Treasury bills (0.8%) and the risky rate as the return on U.S. stocks (7.4%). This choice for the safe rate is not too bad as one can argue that the relevant safe return for the rest of the world is not that far off from the return on U.S. Treasury bills. And, it is difficult to find a figure for the global risk-free rate. Since U.S. assets take up more than 70% of the MSCI World Index, it is perhaps not too bad to follow Pindyck and Wang (2013) and use this figure of 7.4%. The *global* return on risky assets may be 0.2% lower than the U.S. return due to the higher return in emerging markets, so the effect on the coefficient of relative risk aversion and the elasticity of intertemporal substitution will be very small. For the sake of consistency we therefore stick to the returns on safe and risky assets used in Pindyck and Wang (2013) and other papers including van den Bremer and van der Ploeg (2021).

Following the calculations in Pindyck and Wang (2013) but taking leverage into account one obtains a non-linear system that involves five equations and five unknowns $A^*, \varphi, \delta_k, \delta, \gamma$. For the risk-free rate and the risk premium, one obtains

$$r^f = \delta + \frac{\overline{\mu}}{\psi} - \tfrac{1}{2}\gamma\Big(1+\frac{1}{\psi}\Big)\sigma^2 - \lambda_e\Big(\frac{\alpha_e}{\alpha_e-\gamma+1}\frac{1/\psi-\gamma}{1-\gamma} - \frac{\alpha_e}{\alpha_e-\gamma}\Big), \tag{C.1}$$

$$r^p = \phi\gamma\sigma^2 + \lambda_e\gamma\Big[\frac{\alpha_e}{\alpha_e-\gamma} - \frac{\alpha_e}{\alpha_e-\gamma+\phi} + \frac{\alpha_e}{\alpha_e+\phi} - 1\Big]. \tag{C.2}$$

Given the values of σ, λ_e, and α_e, (C.2) pins down the degree of relative risk aversion γ. Then, (C.1) can be solved for the time preference rate δ. Then, we determine the productivity by

$$A^* = \frac{q}{\chi}\Big[\delta + \Big(\frac{1}{\psi}-1\Big)\Big(\overline{\mu} - \tfrac{1}{2}\gamma\sigma^2 - \frac{\lambda_e}{1-\gamma}\frac{\alpha_e}{\alpha_e-\gamma+1}\Big)\Big]. \tag{C.3}$$

In equilibrium, the model generates an investment-capital ratio of $i = A^*(1-\chi-\eta)$ and Tobin's Q is $q = \frac{1}{1-\varphi i}$. Hence, the adjustment cost parameter φ is given by

$$\varphi = \frac{1-1/q}{i}. \tag{C.4}$$

Finally, the capital depreciation rate δ_k is given by

$$\delta_k = i - 0.5\varphi i^2 - \overline{\mu}. \tag{C.5}$$

We use the above equations to calibrate the remaining preference parameters, the depreciation rate, the investment adjustment cost parameters, and the total factor productivities given in Table 1 to match an expected GDP growth rate of $\overline{\mu} = 2.52\%$ in normal times without disasters (Wachter, 2013), a consumption share of $\frac{C}{Y} = 63\%$ of GDP, a risk-free interest rate of $r^f = 0.8\%$, an equity risk premium of $r^p = 6.6\%$, and a Tobin's Q of 1.548 (Pindyck and Wang, 2013).

Energy Consumption We set the energy shares in the production functions to $\eta_i = 0.043$ (van den Bremer and van der Ploeg, 2021).[42] We set the initial cost of fossil fuel to $b_f(S_0)$ = \$540/tC (cf. van den Bremer and van der Ploeg, 2021), but use a significantly higher initial cost of green energy, $b_g(S_0)$ = \$810/etC, in line with production costs in developed countries. We have learning by doing in the production of renewables as the unit production cost drops by 20% for every doubling of cumulative installed volume of renewables based on a voluminous literature on learning curves in accordance with Swanson's law (e.g. Lafond et al., 2018), hence the cost of green goods drops as the green transition

[42] This assumption is in line with Golosov et al. (2014) who use an energy share of 4%.

progresses.[43] This green technical progress is not exogenous and is an alternative to directed technical change (Acemoglu et al., 2012). We suppose that the cost parameter for green energy gradually declines over time as the green transition progresses by setting $b_g(S_t) = b_g(S_0)k_0(1-S_t)^{-k_1}$ with $k_0 > 0$ and $k_1 > 0$. This gives $k_0 = 0.5107$ and $k_1 = 0.3219$.

The green sector only uses renewable energy, so $\kappa_{1,1} = 1$, $\kappa_{2,1} = 0$, and ρ_1 can be chosen arbitrarily. The brown sector can be fueled by both energy sources. To calibrate the energy composite of the brown sector and the CES weights, we set the elasticity of intratemporal substitution to $\zeta_2 = 2$ corresponding to $\rho_2 = 0.5$ and the CES weights to $\kappa_{1,2} = 0.356$, $\kappa_{2,2} = 0.644$ (Golosov et al., 2014). With this calibration it is possible to fully replace fossil fuel by green energy withing this sector even though moving capital to the green sector may be more efficient.

Given those parameter choices, we determine the share of brown capital such that the model generates 19.77% of renewable energy in total energy demand in the BAU-scenario in 2020.[44] This gives an initial share of brown capital of $S_0 = 0.876$. We can thus back out the initial green and brown capital stocks (74.3 and 1353.9 trillion US $, respectively).

Emission Intensity Since the emission intensity ν follows $\mathrm{d}\nu = \nu_- \left[g_\nu \mathrm{d}t - \frac{\mathrm{d}K}{K_-} \right]$, industrial emissions are given by $E_t^{ind} = (f_{1t}(1-S_t) + f_{2t}S_t)K_0 \mathrm{e}^{\int_0^t g_\nu(s)\mathrm{d}s}$. In the BAU state, the social planner does not take account of the negative externalities caused by emissions but reallocates capital from the brown to the green sector for other reasons such as diversification purposes (e.g. Hambel et al. (2024) and the references therein). We now solve and simulate the pure BAU scenario over the next 100 years assuming a reallocation cost parameter of $\kappa = 2$. This parameter choice yields a BAU simulation of temperature, emissions, and energy that is well in line with the adjusted RCP8.5 scenario. Given the adjusted RCP8.5 emission data E_t and the simulated share of brown capital S_t, we approximate $p(t) = \frac{E_t}{\mathbb{E}[f_{1t}(1-S_t)+f_{2t}S_t]}$ by a cubic polynomial function of time, $p(t) = p_0 + p_1 t + p_2 t^2 + p_3 t^3$, with $p_0 = 2.08 \cdot 10^{15}$, $p_1 = 4.22 \cdot 10^{13}$, $p_2 = 1.01 \cdot 10^{12}$, $p_3 = -9.76 \cdot 10^9$, and $R^2 > 99\%$. The corresponding growth rate g_ν is then given by $g_\nu(t) = \frac{\mathrm{d}}{\mathrm{d}t} \ln p(t)$. Figure C.1 depicts the adjusted RCP8.5 emission data and the model fit. Panel (a) shows the simulated data $p(t)$ (o) determining the emission intensity and its cubic fit. Panel (b) depicts the median evolution of the BAU emissions (——) and compares it to the RCP8.5 emission predictions (o). It also shows the corresponding 5% and 95% quantile of BAU emissions (- - -). This calibration implies that the emission intensity ν_t tends to decline over time although it is exposed to stochastic shocks.

[43] Swanson's law is the solar industry specific application of Wright's Law which states there will be a fixed cost reduction for each doubling of manufacturing volume. More specifically, Swanson's law states that the price of solar panels drops by 20 percent every time the volume of panels shipped doubles, see https://www.economist.com/news/2012/11/21/sunny-uplands.

[44] We use world bank data on the share of renewable energy of total final energy consumption, see https://data.worldbank.org/indicator/EG.FEC.RNEW.ZS.

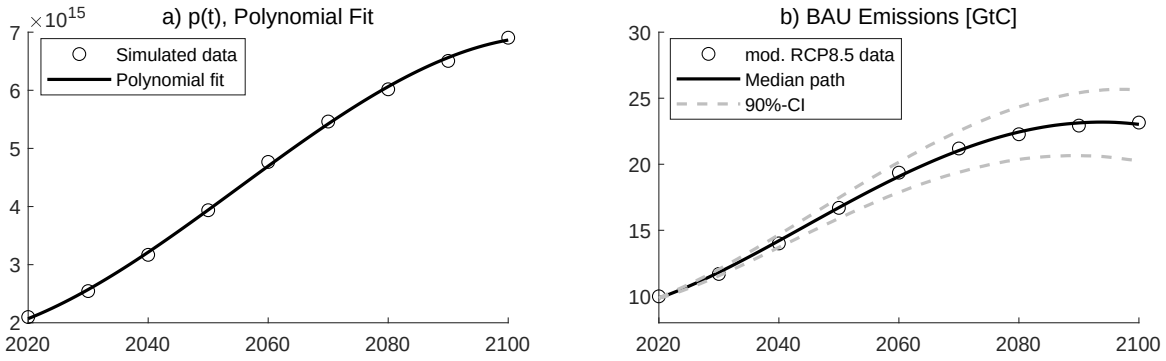

Figure C.1: Calibration of Emission Intensity. Panel (a) shows the simulated data $p(t)$ (o) determining the emission intensity and its cubic fit. Panel (b) depicts the median evolution of the BAU emissions (——) and compares it to the adjusted RCP8.5 emission data (o). It also shows the 5% and 95% quantiles of BAU emissions (- - -).

We thus calibrate the emission intensity such that the pure BAU simulation mimics the modified RCP8.5 scenario of the Fifth Assessment Report of the Intergovernmental Panel on Climate Change (Cambridge University Press, 2014). RCP8.5 is characterized by high emissions leading to a temperature increase of about 4.3°C relative to the pre-industrial level by the end of this century.[45] We slightly modify the emission data to take account of the lower emissions in reality compared to the RCP8.5 scenario. While the scenario predicts emissions of 12.44 GtC in 2020, emissions were only 10 GtC. Thus, we calibrate the emission intensity to adjusted RCP8.5 emission data that is 20% lower than the original data.

Temperature Dynamics Estimates of the transient climate response to cumulative emissions range from 0.8 to 2.4°C/TtC (e.g. Allen et al., 2009; Matthews et al., 2009). We take a TCRE of $\vartheta = 1.8$°C/TtC, which is in line with the temperature evolution in DICE-2016R and other climate-economic models such as Dietz and Venmans (2019). Moreover, we choose a constant temperature volatility of $\sigma_T = 0.033$ to match the temperature range of global mean temperature increase in the RCP scenarios.[46]

Damage Specification We use a standard, inverse quadratic damage function of the form $\Lambda(T) = \frac{1}{1+\theta T^2}$. The damage function parameter corresponding to Nordhaus (2017) is $\theta = 0.00236$. This leads to very low carbon taxes, and a prominent recent study suggests that damages are much higher leading to a benchmark SCC of around \$185/tCO$_2$, see Rennert et al. (2022).[47] Tol (2023) has conducted a meta

[45] The data is available from the RCP database, see `http://tntcat.iiasa.ac.at/RcpDb`.

[46] The temperature range in the year 2100 of the various RCP scenarios varies between 0.8°C around its mean in RCP2.6 to 1.1°C in RCP8.5.

[47] Bilal and Känzig (2024) obtain an even higher benchmark SCC of around \$1,000/tCO$_2$. We do not adopt this higher value, but will in Section 5 allow for temperature-dependent risks of climate disasters which pushes up the SCC considerably.

analysis and found that the estimates of the SCC have increased considerably. He finds an average SCC of about \$40/tCO$_2$ for a low discount rate corresponding to a market based-calibration although the SCC can easily reach three-digit numbers for lower discount rates. Since our calibration is market-based, we calibrate the damage parameter to match the \$40/tCO$_2$ in 2020, leading to $\theta = 0.0073$.[48]

C.2 Additional Calibration Details for Extended Model

Climate Tipping Risks Given the initial value of the TCRE in the pre-tip state, $\vartheta(X_0^c = 1) = 1.8^\circ\text{C/TtC}$, and the range of estimates up to 2.4°C/TtC for the TRCE, we choose a TCRE of $\vartheta(X^c = 2) = 2.1^\circ\text{C/TtC}$ for the intermediate state and $\vartheta(X^c = 3) = 2.4^\circ\text{C/TtC}$ for the post-tip state. From the pre-tip state, the transition intensity to the intermediate and post-tip state is $\lambda_c(\mathbf{S}, 1, j) = \widehat{\lambda}_c^{1,j}(T-1)$ with $\widehat{\lambda}_c^{1,j} = 0.012$ (cf. Cai and Lontzek, 2019).[49] This implies an annual initial tipping intensity of 0.324% at $T_0 = 1.27^\circ\text{C}$ corresponding to an expected duration of 309 years and a tipping intensity of 1.2% at $T = 2^\circ\text{C}$ corresponding to an expected duration of 83 years. The transition intensity for the post-tip state conditional on being in the intermediate state is $\lambda_c(\mathbf{S}, 2, 3) = \widehat{\lambda}_c^{2,3} = 0.02$ corresponding to an average duration of 50 years between the intermediate and the final climate tipping state. The climate can also jump directly from state 1 to state 3, so the total tipping intensity at the initial temperature $T_0 = 1.27^\circ\text{C}$ is 0.648% (cf. van den Bremer et al., 2023). Finally, we have irreversible climate tipping, so $\lambda_c(\mathbf{S}, i, j) = 0$ for $j < i$.

Negative Emission Technology For the calibration of the parameters of the marginal cost function for the negative emission technology $\frac{\partial b_d(S, X^t=2, D, K)}{\partial D} = K[a_1(S) + a_2(S)a_3(S)\exp(a_3(S)D)]$, we first average the data from the two scenarios described in Rebonato et al. (2023) and shown in their Figure 5. We neglect the very small share with low but steep marginal costs for removal that is close to zero. The averaged data—expressed in GtC—is depicted in Figure C.2 for the year 2050 (Panel a) and 2100 (Panel b). Then, we calibrate the truncated power functions of the form $a_j(S) = b_j \max(\zeta, S)^{c_j}$, $j \in \{1,2,3\}$ jointly to both curves by assuming that the time dependencies are only driven by variations in S. In this sense, S models technological progress towards a low-carbon economy. We simulate S and K for the optimal scenario (PIGOU) and calibrate the power functions a_1, a_2, a_3 such that the expected marginal costs at $\tau \in \{31, 81\}$, i.e., in the years 2050 and 2100, respectively, match the marginal cost curves as closely as possible in a least-squares sense. The parameters obtained are all strictly positive so that in particular $\frac{\partial^2 b_d(S, X^t=2, D, K)}{\partial D \partial S} > 0$, i.e., the greater the proportion of brown capital, the greater the marginal removal costs. The fit is visualized by the black line (——). The exponential marginal cost function performs very well with an R^2 exceeding 99%.

[48] This carbon price is computed along the optimal Pigouvian path without policy uncertainty (see Appendix E.3). With temperature-dependent risks of recurring climate disasters and climate tipping (see section 5), it becomes \$113/tCO$_2$.

[49] Climate tipping is only possible if temperature exceeds 1°C, which given our initial temperature is the case.

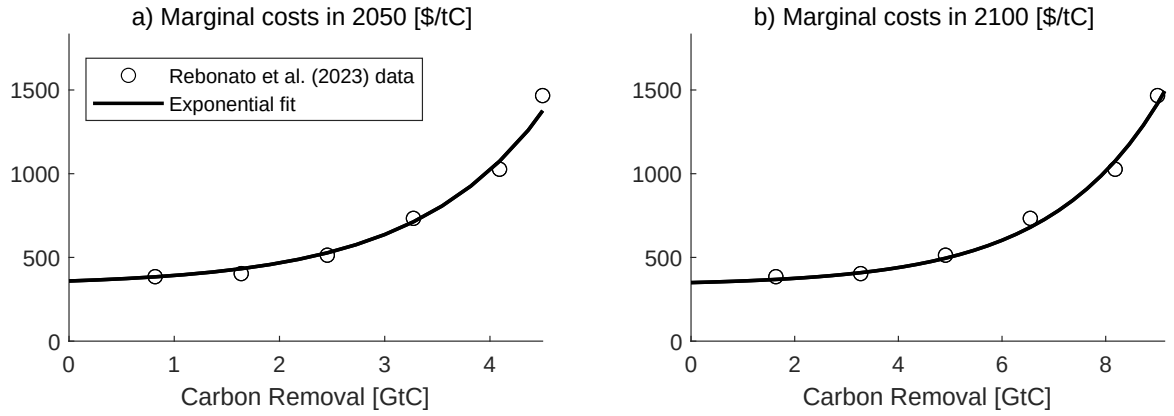

Figure C.2: Calibration of the Marginal Cost Function for NET. The figure shows the averaged data from the two scenarios in Rebonato et al. (2023) (o). Panel (a) shows the resulting marginal costs function for the year 2050 and Panel (b) for the year 2100, respectively. We fit an exponential function of the form $\frac{\partial b_d(S,X^t=2,D,K)}{\partial D} = K[a_1(S)+a_2(S)a_3(S)\exp(a_3(S)D)]$ to this data as shown by the black line (——), where $a_j(S) = b_j \max(\zeta,S)^{c_j}$ are truncated power functions of the share of brown capital.

More Realistic Model of Policy Tipping Ongoing global warming (exponentially) increases the likelihood of strengthening climate policy once temperature has crossed 1.5°C (Barnett, 2024). Although carbon taxes or cap-and-trade systems have never been completely abolished after they had been implemented, there is a significant hazard of climate change deniers coming (back) to power. To allow for transitions back to BAU, we model political transition intensities by

$$\lambda_p(\mathbf{S},i,j) = \widehat{\lambda}_p^{i,j} \exp\left(\widehat{\mu}[\max(T-1.5,0)-S]\right), \qquad i<j$$
$$\lambda_p(\mathbf{S},i,j) = \widehat{\lambda}_p^{i,j} \exp\left(\widehat{\mu}[\min(1.5-T,0)+S]\right), \qquad i>j$$

with $\widehat{\lambda}_p^{i,j} > 0$ for $i \neq j$ and $\widehat{\mu} > 0$. The probability for jumps to a more ambitious climate policy ($j > i$) thus rises in temperature if $T > 1.5$°C. It also falls in the share of brown capital as a result of lobbies to slow down the green transition;[50] also, as the green sector grows in size, green lobbies increase the chance of more stringent climate policies. Conversely, the probability for jumps back to a less ambitious climate policy ($j < i$), falls in temperature if $T > 1.5$°C and rises in the share of brown capital due to stronger brown and weaker green lobbies.

We choose parameters to roughly match the likelihood and resulting temperature increase of the various transition scenarios in Moore et al. (2022): about 48% of their simulations are in their modal scenario, which leads to an average temperature increase of 2.3°C. About 28% of their simulations lead to ag-

[50] For instance, more than 2400 lobbyists affiliated with oil and gas industries attended the recent climate summit COP28, e.g. https://www.theguardian.com/environment/2023/dec/05/record-number-of-fossil-fuel-lobbyists-get-access-to-cop28-climate-talks.

gressive climate action limiting global warming to up to 1.8°C. There is less ambitious or less effective climate action in the remaining scenarios (about 24%) with average temperature increases of around 3°C, of which less than two percent of the simulations lead to significantly higher temperatures. To replicate those figures with our model, we use the parameterization in Table 2. We thus find that the jump intensity from BAU to modest (PIGOU) or ambitious (CAP) climate policies at $T_0 = 1.27$°C and $S_0 = 0.876$ is 6.22% and 2.59%, respectively, which correspond to an expected duration of 16.08 or 38.56 years. The average time until the government takes climate action is half the harmonic mean of those average durations: 11.35 years. Compared to technological or climate tips, these are quick transitions. If BAU continues and temperature rises to say 2°C, expected durations shorten to 11.05 and 26.52 years, respectively. This cuts the average time until the government takes climate action to 7.80 years. Hence, we assume that ongoing global warming and a smaller share of brown capital make it more likely that policy makers start taking the climate serious.

D Additional Simulation Results for the Core Model

This section provides further details including the policy functions for the simulations of our core model.

D.1 Scenarios without Transition Risks.

Macroeconomic outcomes and temperature for the BAU and CAP policy simulations are presented in Figure D.3. As can be seen from Figure D.4, the risk-free rate and the risk premiums are hardly affected in this BAU scenario. This is in line with van den Bremer and van der Ploeg (2021), Hambel et al. (2024), who demonstrate that TFP damages alone are not sufficient to generate a *temperature risk premium* in the spirit of Bansal et al. (2017), Donadelli et al. (2017), Hong et al. (2019), and Gregory (2024). We therefore extend the model with climate-related disaster and climate tipping risks in section 5.

D.2 Policy Functions for the Core Model

Here we discuss the influence of the state variables and the policy states on the optimal decisions and asset returns, captured by the so-called policy functions. From this, we derive intuition for the influence of the share of brown capital and temperature on the optimal controls. In particular, we discuss how climate change affects the interest rate and asset returns. All the results are for the benchmark calibration of our core model for the year 2025. The policy functions are depicted in two figures and depend on the state variables, i.e. S, T and X^p. They are qualitatively similar for other years. Figure D.5 depicts policy functions for the BAU policy state, and Figure D.7 for the CAP policy

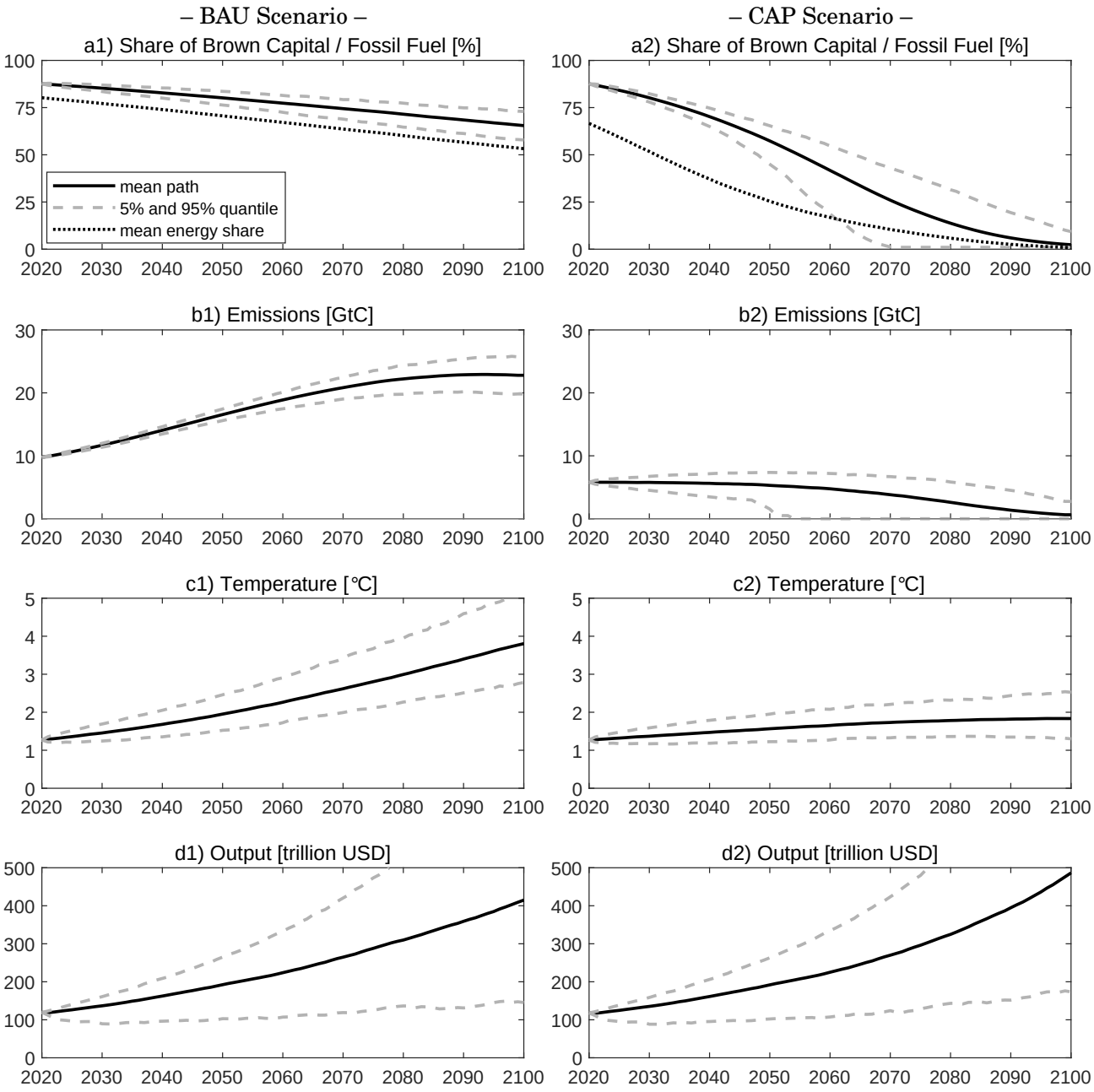

Figure D.3: BAU Scenario (left panels) and CAP scenario (right panels) without Transition Risks. Mean values are depicted by solid lines (——) and 5% and 95% quantiles by dashed lines (- - -). The dotted lines (·····) in Panels a1) and a2) depict the mean path of the share of fossil fuel in the global energy mix.

state. The dark lines (——) depict $S = 0.75$, the gray lines (——) refer to S = 0.5, and the light lines (——) to S = 0.25. The horizontal axis depicts the temperature in the range from 0°C to 4°C.

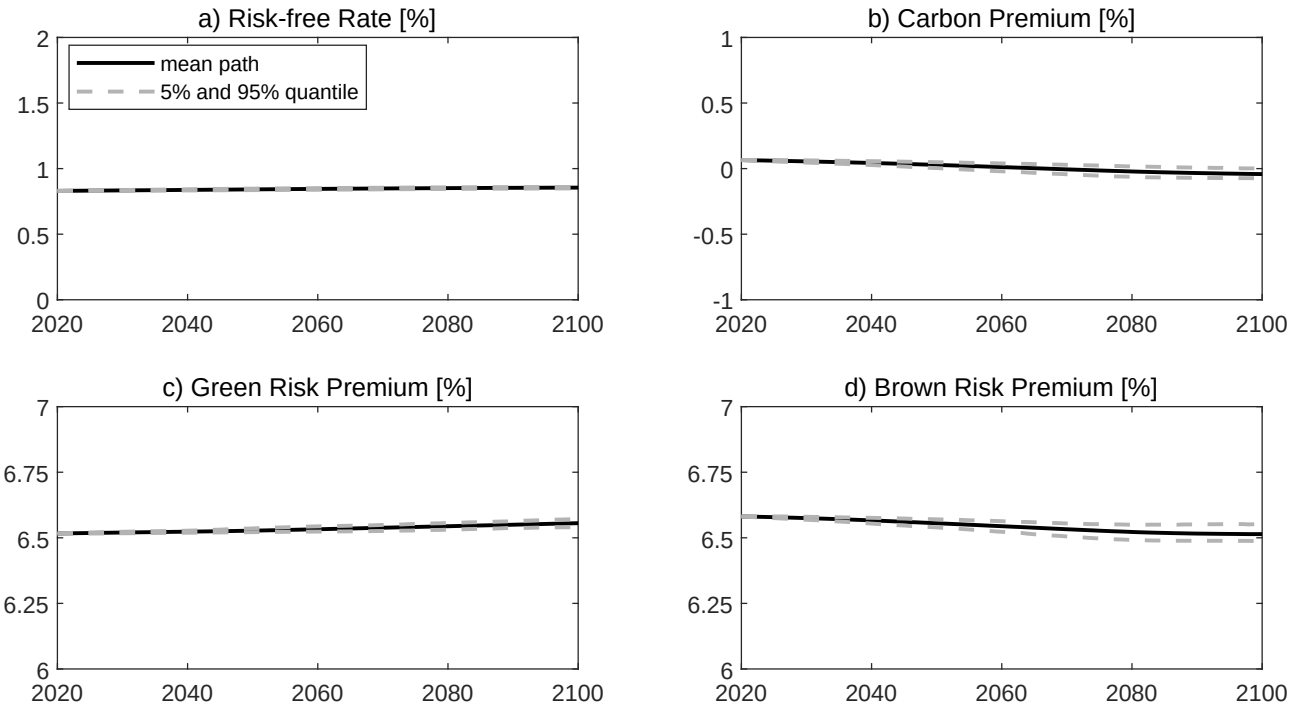

Figure D.4: Business-as-usual Scenario without Transition Risks: Asset Pricing. Average values are depicted by solid lines (——) and 5% and 95% quantiles by dashed lines (- - -). The dotted line (·····) in panel a) depicts the mean path of the share of fossil fuel in the global energy mix.

BAU Policy State Panel a) of Figure D.5 shows that in the BAU policy state the carbon tax is zero (panel c)). Optimal consumption hardly depends on the share of brown capital although it is high if the share of green capital is high. Panel b) depicts optimal capital reallocation from the brown sector to the green sector. As policy makers ignore the negative externality from carbon dioxide but has a motive for diversification, they reallocate capital from the brown to the green sector only if the capital share is above 50% (Hambel et al., 2024). The relocation does not depend on temperature in the BAU state. Panels d), e), and f) depict energy use relative to the respective capital stock, which does not vary with temperature, but brown energy is high and green energy use is low if the share of brown capital is high.

Since capital markets price in climate transition risks and anticipate both climate damages and potential climate policy that may eventually be implemented, the asset pricing moments depicted in panels g), h), and i) depend on temperature. Panel g) shows that the risk-free rate decreases in the share of brown capital and is heavily curbed for temperatures above the two degrees cap. If a policy shock from the BAU to the CAP policy state would hit the economy when temperatures are above the 2°C cap, the brown capital stock may not be operated anymore. This policy transition risk is priced in (see equation (3.2) and the discussion in the main text). Similar effects lead to a slight increase of the risk premiums of both risky assets around the critical temperature of two degrees, leading to a transition risk premium

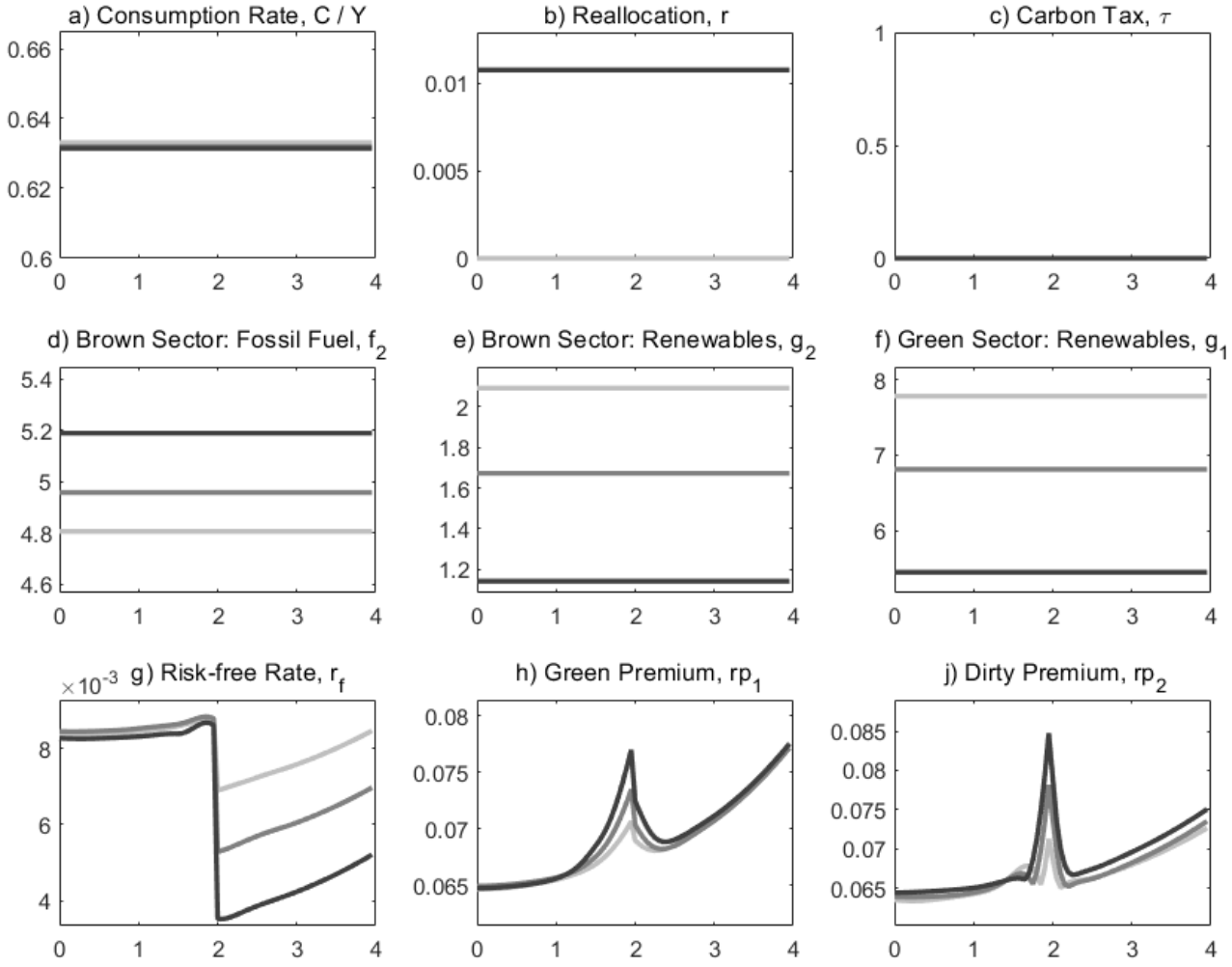

Figure D.5: Policy Functions for the BAU Policy State. The graphs depict policy rules as functions of the two state variables S and T and of the policy state. On the horizontal axis is temperature in the range 0°C to 4°C. The lines represent various levels of the brown capital share: dark lines (——) depict $S = 0.75$ the gray lines (——) refers to $S = 0.5$, and the light lines (——) to $S = 0.25$.

in the spirit of Engle et al. (2020). These transition risks are more pronounced if the share of brown capital in the total capital stock is large.

CAP Policy State Turning to the CAP policy state, Panel a) of Figure D.7, shows that the consumption-to-output ratio significantly increases when temperatures exceed 2°C. Because from then on fossil fuel must not be used anymore (panel d)), output and economic growth drop. This effect is more pronounced if the share of brown capital is large and society relies more on fossil fuel. The economy satisfies its desire for consumption smoothing by increasing the consumption-to-output ratio and the demand for renewable energy in the brown sector that can partially substitute fossil fuel (panel e)). Panel b) il-

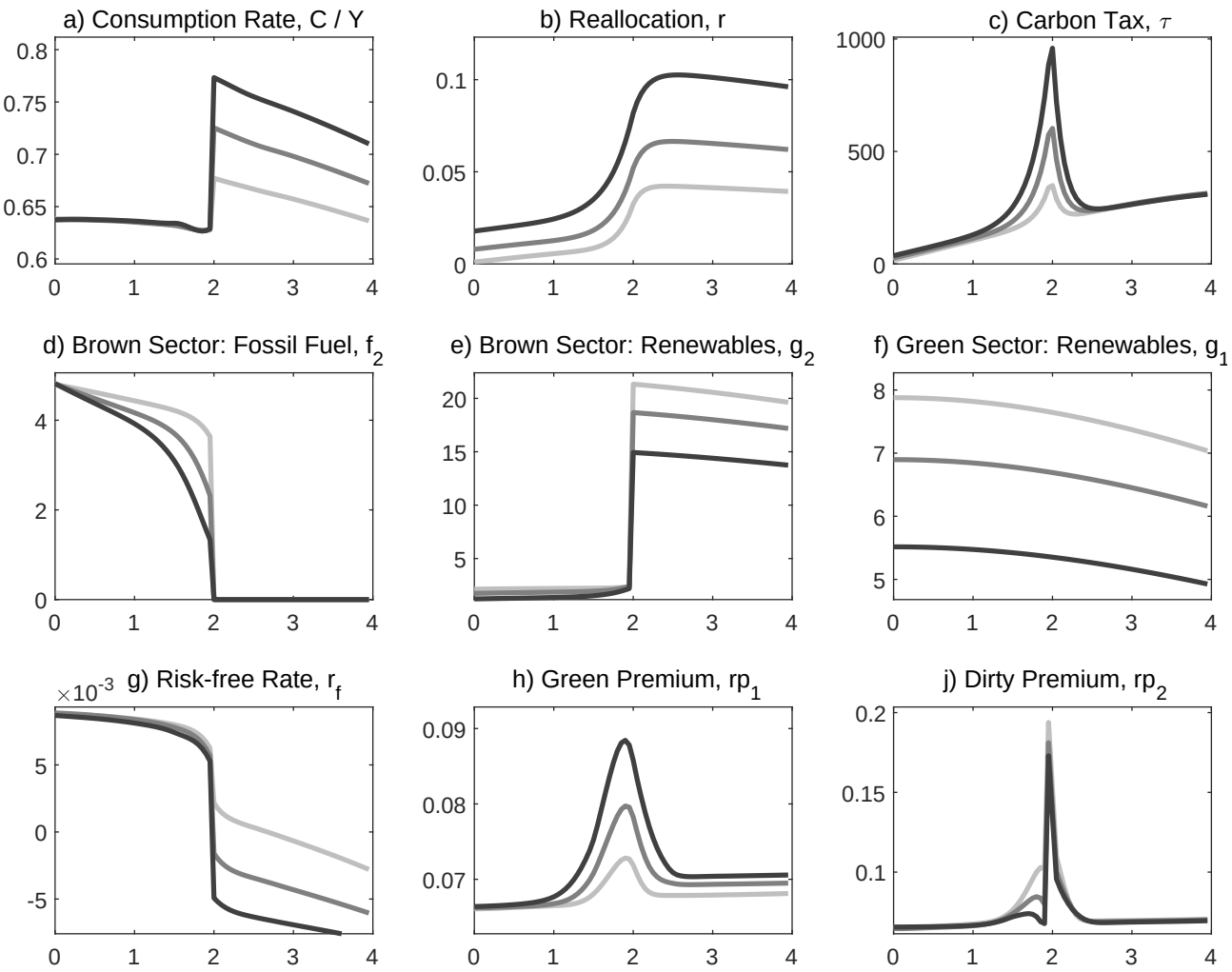

Figure D.6: Policy Functions for the CAP Policy State. The graphs depict policy rules as functions of the two state variables S and T. On the horizontal axis is temperature in the range 0°C to 4°C. The lines represent various levels of the brown capital share: dark lines (——) depict $S = 0.75$, the gray lines (——) refers to $S = 0.5$, and the light lines (——) to $S = 0.25$.

lustrates that capital reallocation takes place at a much faster rate than in the BAU state. Due to prevailing climate risks and policy, society keeps on reallocating even if the share of brown capital is already quite low. Panel c) illustrates that the carbon tax increases dramatically if temperatures are close to but still below two degrees in order to prevent them from crossing the cap. Once temperatures exceed the 2° cap, it becomes more and more unlikely that they will fall below 2° again. Thus for high temperatures, the carbon tax is merely a shadow price as carbon dioxide must not be emitted anymore.

Panel g) depicts the equilibrium risk-free rate. As in the BAU policy state, it drops drastically if temperatures are below two degrees. This is, however, not due to the jump component in equation (3.2), which is zero in the CAP policy state. This drop is mainly driven by the consumption smoothing component

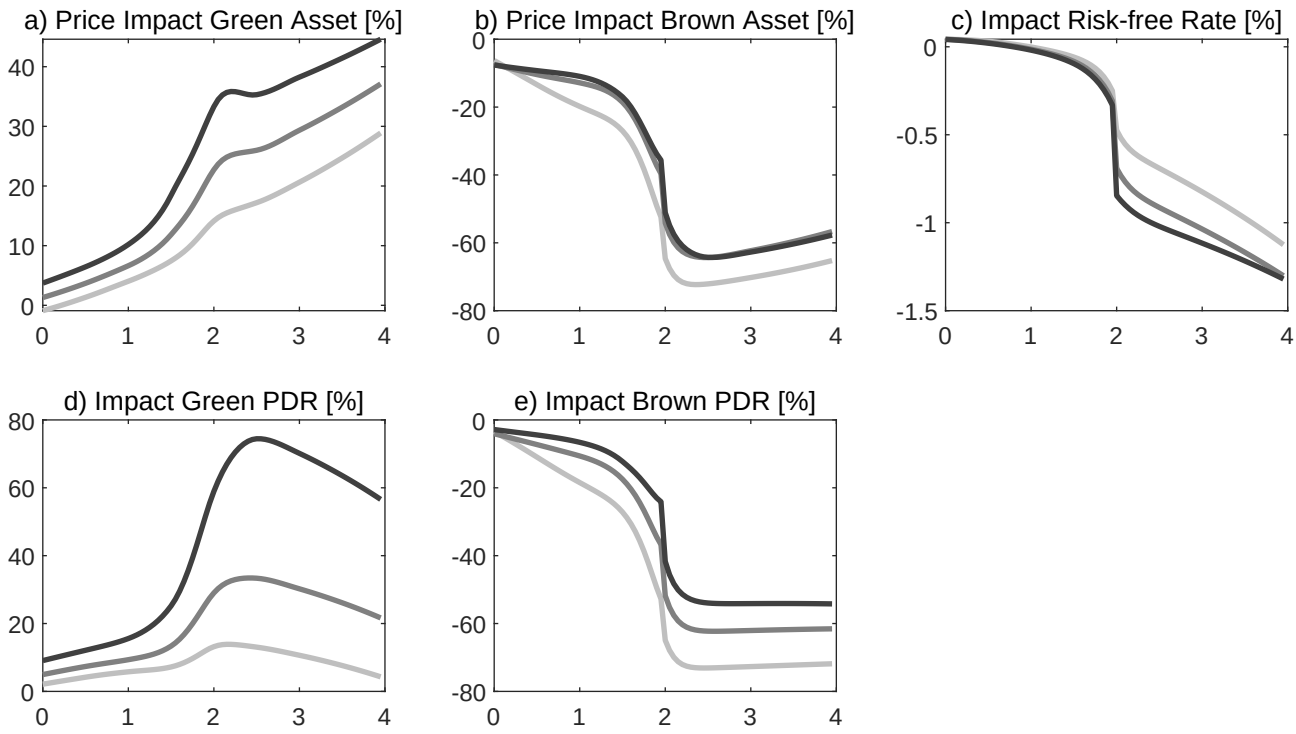

Figure D.7: Effect of Climate Policy on Financial Markets. The graphs depict the effect of a transition from the BAU state to the CAP policy state as functions of the two state variables S and T. On the horizontal axis is temperature in the range 0°C to 4°C. The lines represent various levels of the brown capital share: dark lines (——) depict $S = 0.75$, the gray lines (——) refers to $S = 0.5$, and the light lines (——) to $S = 0.25$.

$\frac{1}{\psi}\mu_C$. As fossil fuels must not be used anymore, the expected consumption growth rate is much lower than in the BAU state. Consequently, the risk-free rate experiences a negative shock, which is stronger if the economy relies a lot on brown capital. Finally, panels h) and i) depict the risk premiums of the two risky assets. Again, both assets price in the aforementioned transition risk, which corresponds to the first line of (B.13). Now the brown asset is much stronger affected than the green asset, leading to a positive carbon premium (see the second line of (3.4) and the discussion in the main text).

Effect of Climate Policy on Financial Markets We now examine the impact of a policy transition from the BAU to the CAP policy state. It turns out that such a policy transition has significant implications for financial markets. As can be seen from panels a) and b), the price of the green asset goes up drastically while the price of the brown asset is negatively affected. While the impact of such a policy shock is rather moderate for low temperatures, it increases drastically if temperatures are close to or above two degrees. The stark negative price effect on the brown asset is particularly pronounced if the temperature cap has been crossed and fossil fuel must not be used for production anymore. We also see that the positive price impact on the green asset is stronger if there is still much brown capital in

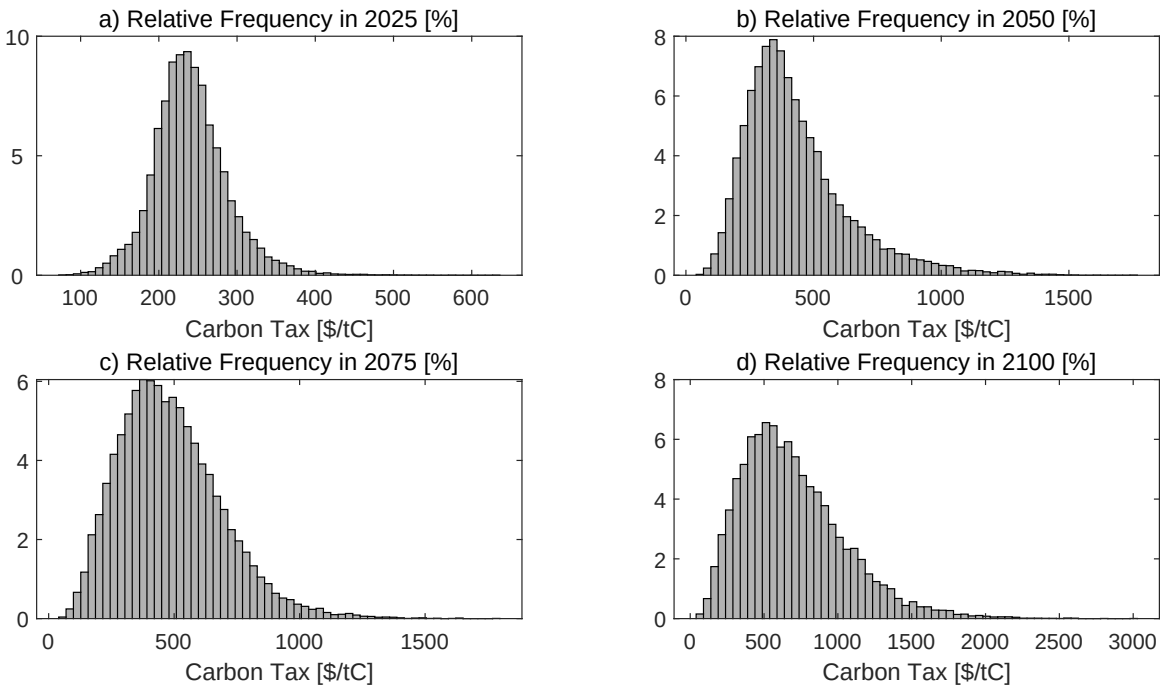

Figure D.8: Carbon Taxes. The figure shows histograms for the implemented carbon tax, i.e., conditional on being in the CAP policy state, for the years a) 2025, b) 2050, b) 2075, and d) 2100.

the economy. Then, the demand for green assets to compensate the loss in the brown sector is particularly strong. These findings are also reflected in panels e) and f), which illustrate the effect on the price-dividend ratios of both risky assets.

Panel c) now illustrates the effect of a policy transition shock on the risk-free rate, which is always negative. If temperatures are below the 2° cap, the risk of phasing out fossil fuel is now more pronounced and so the demand for precautionary savings increase. If temperatures are already above two degrees, production becomes more expensive as fossil fuel must not be used anymore. Consequently, consumption growth is slowed down and the term $\frac{1}{\psi}\mu_C$ in equation (3.2) becomes smaller after the policy transition.

D.3 Additional Material for the Core Simulations

Optimal Carbon Taxes Table D.1 reports the unconditional moments of the implemented carbon tax for the years 2025, 2050, 2075, and 2100. Since the carbon tax is implemented in only about 25% of the paths in 2025, its unconditional distribution is clearly right-skewed. Its skewness tends to decline over time as carbon taxes are implemented in more and more paths. Figure D.8 shows histograms for implemented carbon taxes for the years 2025, 2050, 2075, and 2100. Those histograms are generated with 20,000 paths conditional on being in the CAP policy state.

(a) Unconditional moments

	$\mathbb{E}[\tau]$	$\text{Med}(\tau)$	$\sigma(\tau)$	$q_{5\%}(\tau)$	$q_{95\%}(\tau)$	$\text{Skew}(\tau)$
2025	42	0	97	0	275	2.01
2050	372	345	366	0	1072	1.06
2075	465	457	300	0	957	0.74
2100	696	651	395	0	1402	0.65

(b) Conditional moments

	$\mathbb{E}[\tau]$	$\text{Med}(\tau)$	$\sigma(\tau)$	$q_{5\%}(\tau)$	$q_{95\%}(\tau)$	$\text{Skew}(\tau)$
2025	254	250	53	175	347	0.70
2050	562	481	309	215	1197	1.48
2075	538	501	254	210	989	1.48
2100	738	677	367	247	1416	0.93

Table D.1: Optimal Carbon Tax. The table reports summary statistics of (a) the unconditional optimal carbon tax and (b) the optimal carbon tax conditional on being implemented for the years 2025, 2050, 2075, and 2100.

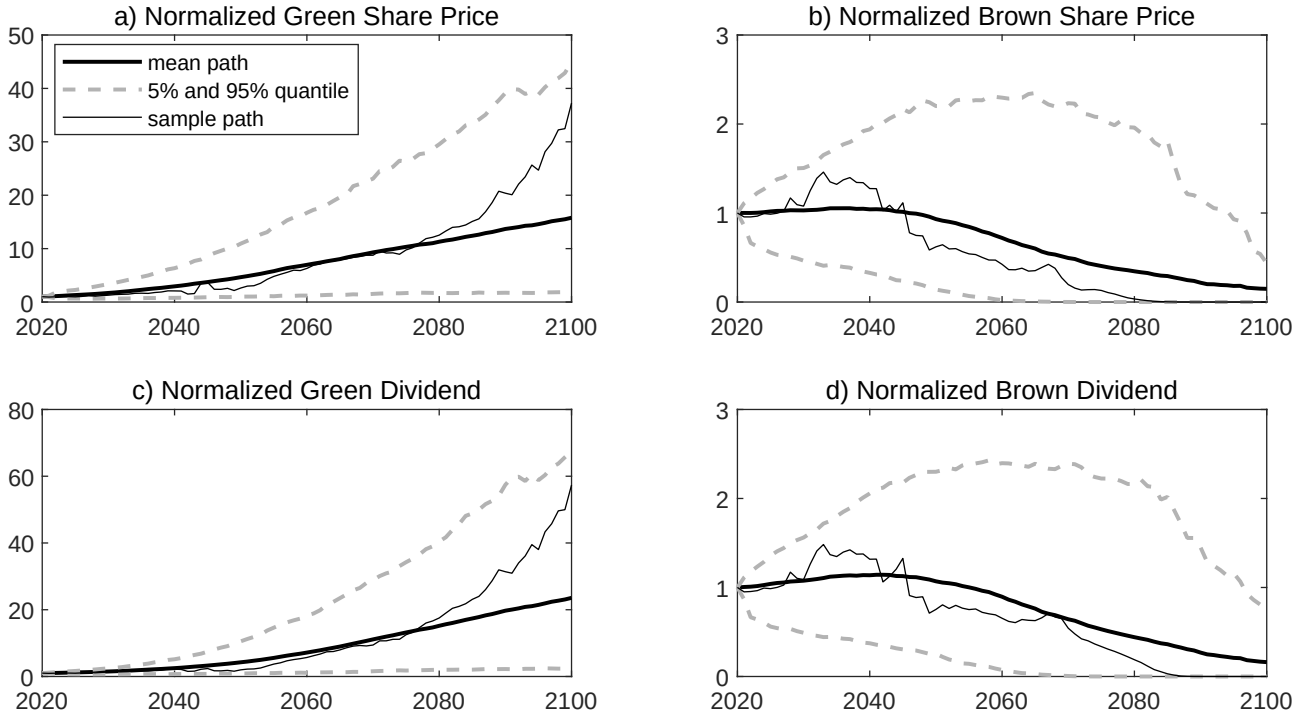

Figure D.9: An Illustrative Sample Path (Asset Prices). Average values are depicted by solid lines (——) and 5% and 95% quantiles by dashed lines (- - -). To simplify the comparison between the brown and green assets, we have normalized share prices in 2020 in panels (a) and (b) and dividends in 2020 in (c) and (d) to one in each case. The thin black lines (——) shows one illustrative sample path, where society switches from the BAU policy state to the CAP policy state in the year 2045.

An Illustrative Sample Path for Asset Prices Figure D.9 complements Figure 2 from the main text. In particular, it illustrates the simulated normalized dividends and share prices for both risky assets. Panels a) and b) illustrate the price impact of a climate policy shock from the BAU state to the

Scenario		Average Carbon tax [$/tCO$_2$]				Carbon premium [%]			
	λ_x	2025	2050	2075	2100	2025	2050	2075	2100
BAU	–	0	0	0	0	0.0	0.0	0.0	0.0
PIGOU	–	45	77	127	199	–0.1	0	0.2	0.6
CAP	–	66	117	132	190	–0.5	0.3	2.0	1.8
BAU → CAP	4%	11 (73)	99 (153)	122 (143)	190 (202)	–0.2	0.3	1.6	1.1
BAU → CAP	20%	45 (72)	129 (129)	134 (134)	195 (195)	–0.5	0.5	2.2	2.0
BAU → PIGOU	4%	8 (46)	54 (81)	119 (137)	207 (219)	0.0	0.0	0.1	0.4

Table E.2: SCC and the Carbon Premium in Alternative Scenarios. The table reports average carbon taxes and average carbon premiums or the years 2025, 2050, 2075, and 2100. The numbers in brackets refer to the average optimal carbon tax *conditional* on being implemented.

CAP state in the year 2045. This event is accompanied by a rise in the price of the green asset and a sharp fall in the price of the brown asset. The effect on prices is stronger than on dividends, whereby the price-dividend ratio of the green asset increases strongly and that of the brown asset decreases. The sharp rise in the price-dividend ratio of the green asset causes a decline in the dividend yield. However, the onset of climate policy will increase demand for the green asset in the long term, causing the expected growth rate to rise sharply. This overcompensates for the decline in the dividend yield and leads to an increase in the green premium. Conversely, the increase in the brown risk premium can be explained by the now significantly increased risk of fossil fuels phasing out.

E Sensitivity of Core Results

E.1 Higher Transition Risk

We first examine the extent to which the carbon premium and the carbon tax depend on transition probabilities (see rows 4 and 5 of Table E.2). With an annual transition probability of 20% (rather than 4%) for switching to the CAP policy state, the unconditional average carbon tax is higher because more paths will implement climate policy. It is significantly higher in the short than in the long run, since over time more and more paths will have switched to the CAP policy state and the difference in carbon taxes diminishes. The unconditional average carbon tax is smaller than in the benchmark case as climate action has started earlier and policy makers do not have to catch up on so much that was missed in the BAU policy state. The carbon premiums are higher too in later years.

E.2 Tighter Temperature Cap

The second sensitivity exercise is to examine a temperature cap of 1.5°C instead of 2°C (see Appendix E.4 and Figure E.10). Carbon pricing is then in the next two decades more ambitious to avoid the potentially devastating effects of overshooting the carbon budget, but in the distant future damages and the optimal carbon tax have grown so much that temperature caps no longer bite and the difference in carbon pricing disappears. The carbon premium becomes earlier economically relevant than when the economy is in the CAP state and temperature is close to 1.5°C.

E.3 Carbon Pricing without Temperature Cap

The third sensitivity exercise is to examine what happens if we replace the CAP policy state with a more modest carbon prices called the PIGOU policy state, which internalizes the global warming externalities but does not enforce the temperature cap (see last row of Table E.2). First, consider modest carbon pricing without policy transition risk. In line with the equivalent simulation with the CAP state without transition risk, the carbon premium is initially very small and negative (–0.1%), but remains below 0.75% due to the absence of transition risk. Thus, the magnitude of the carbon premium is small and economically not significant. It only becomes relevant at the end of this century when sizable carbon taxes are implemented.

Second, we consider the scenario with transition risk and the BAU and PIGOU policy states. Simulations starts with BAU until there is a policy switch and policy makers start pricing carbon modestly. Like the BAU and PIGOU scenarios without transition risk, there are no significant carbon premiums. Compared to the PIGOU scenario without transition risk, policy makers implement slightly higher carbon taxes after a transition to the PIGOU policy state to make up for the omitted carbon pricing in the BAU policy state. For instance, in the year 2050, the average carbon tax in the PIGOU policy state is \$81/tCO_2, which is slightly higher than in the pure PIGOU scenario (\$77/tCO_2).

Hence, the risk of exceeding a temperature cap, not policy transition risk, is at the root of a sizeable carbon premium. In this sense, the risk of exceeding a temperature cap is a form of transition risk.

E.4 CAP Scenario without Policy Transition Risks

Figure E.12 provides the simulation results when the model starts in the CAP state and excludes policy transitions to the BAU or PIGOU state (i.e. with the political Markov chain switched off). In contrast to the PIGOU scenario, the carbon premium can be sizable if temperatures are close to 2°C. This scenario leads to an even faster transition to net zero than the PIGOU scenario and policy makers implement more stringent carbon prices.

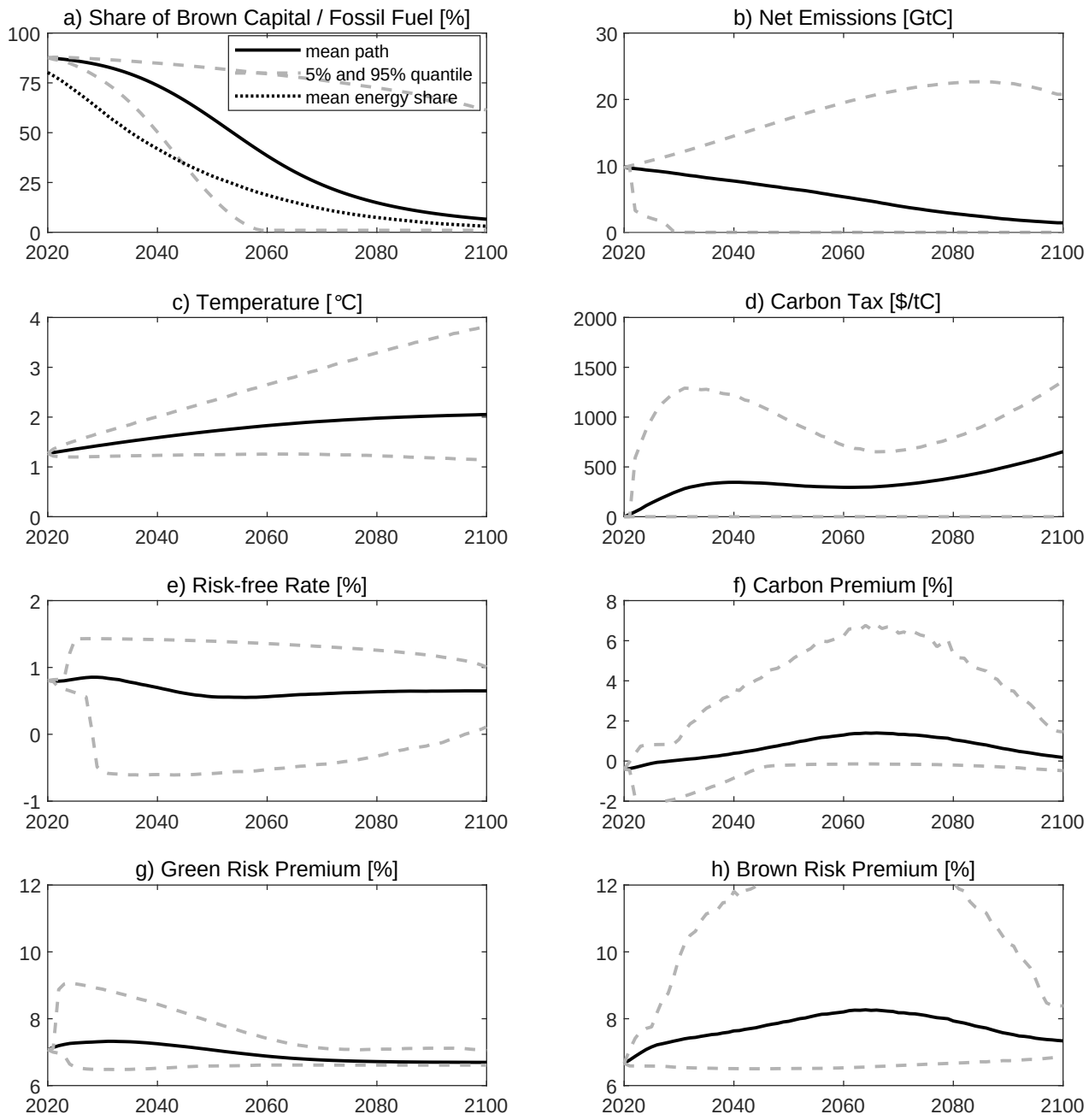

Figure E.10: Core Model with a Tighter Carbon Budget. Average values are depicted by solid lines (——) and 5% and 95% quantiles by dashed lines (- - -). The dotted line (·····) in Panel a) depicts the mean path of the share of fossil fuel in the global energy mix.

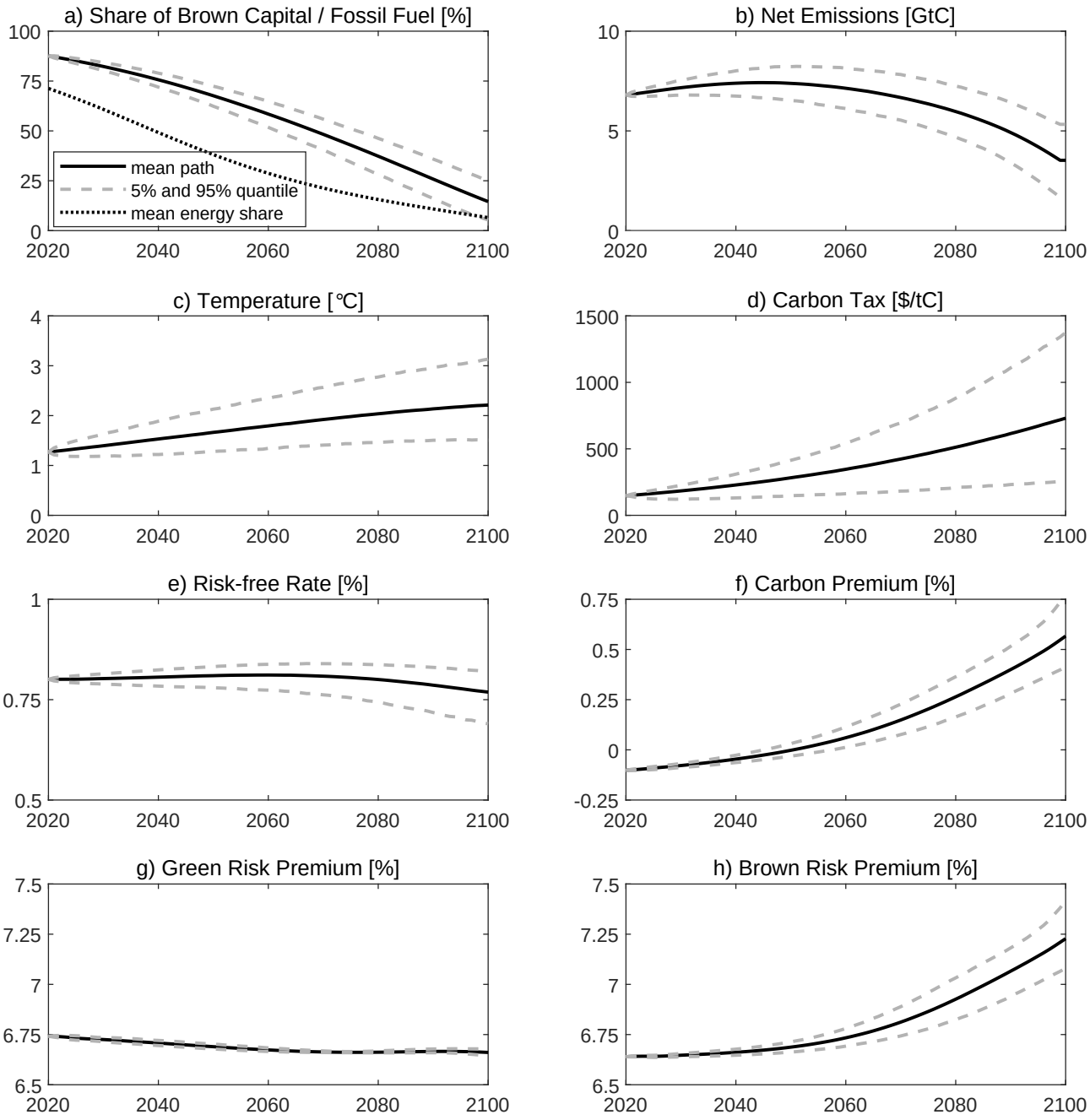

Figure E.11: PIGOU Scenario without Transition Risks (Optimal Carbon Taxes, No Temperature Cap). Average values are depicted by solid lines (——) and 5% and 95% quantiles by dashed lines (- - -). The dotted line (·····) in Panel a) depicts the mean path of the share of fossil fuel in the global energy mix.

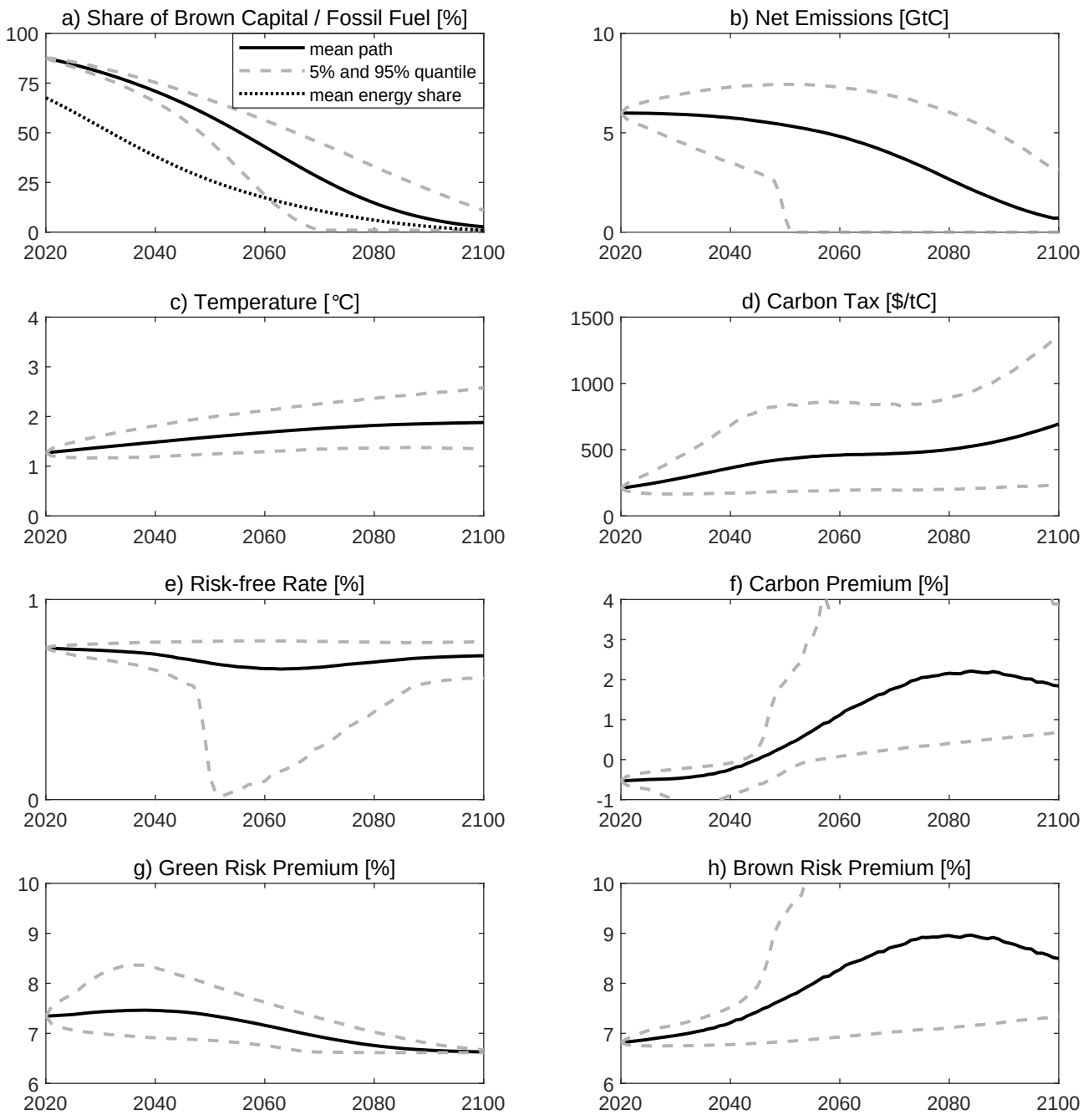

Figure E.12: CAP Scenario without Transition Risks. Average values are depicted by solid lines (——) and 5% and 95% quantiles by dashed lines (- - -). The dotted line (·····) in Panel a) depicts the mean path of the share of fossil fuel in the global energy mix.